EBioMedicine 7 (2016) 35–49

Contents lists available at ScienceDirect

EBioMedicine

journal homepage: www.ebiomedicine.com

Research Paper

Prolactin protects retinal pigment epithelium by inhibiting sirtuin 2-dependent cell death

Rodrigo Meléndez García [a,1], David Arredondo Zamarripa [a,1], Edith Arnold [a,1], Xarubet Ruiz-Herrera [a], Ramsés Noguez Imm [a], German Baeza Cruz [a], Norma Adán [a], Nadine Binart [b], Juan Riesgo-Escovar [a], Vincent Goffin [c], Benito Ordaz [a], Fernando Peña-Ortega [a], Ataúlfo Martínez-Torres [a], Carmen Clapp [a], Stéphanie Thebault [a,*]

[a] Instituto de Neurobiología, Universidad Nacional Autónoma de México (UNAM), Campus UNAM-Juriquilla, 76230 Querétaro, Mexico
[b] Institut National de la Santé et de la Recherche Médicale, U1185, Université Paris-Sud, Faculté de Médecine Paris-Sud, Le Kremlin-Bicêtre 94270, France
[c] Institut National de la Santé et de la Recherche Médicale, U1151, Institut Necker Enfants Malades, Université Paris-Descartes, Faculté de Médecine, Sorbonne Paris Cité, 75014, France

ARTICLE INFO

Article history:
Received 27 January 2016
Received in revised form 23 March 2016
Accepted 31 March 2016
Available online 20 April 2016

Keywords:
Age-related retinal degeneration
Prolactin
Antioxidant
SIRT2
TRPM2 channels
Retinal pigment epithelium

SUMMARY

The identification of pathways necessary for retinal pigment epithelium (RPE) function is fundamental to uncover therapies for blindness. Prolactin (PRL) receptors are expressed in the retina, but nothing is known about the role of PRL in RPE. Using the adult RPE 19 (ARPE-19) human cell line and mouse RPE, we identified the presence of PRL receptors and demonstrated that PRL is necessary for RPE cell survival *via* anti-apoptotic and antioxidant actions. PRL promotes the antioxidant capacity of ARPE-19 cells by reducing glutathione. It also blocks the hydrogen peroxide-induced increase in deacetylase sirtuin 2 (*SIRT2*) expression, which inhibits the TRPM2-mediated intracellular Ca^{2+} rise associated with reduced survival under oxidant conditions. RPE from PRL receptor-null (*prlr*$^{-/-}$) mice showed increased levels of oxidative stress, *Sirt2* expression and apoptosis, effects that were exacerbated in animals with advancing age. These observations identify PRL as a regulator of RPE homeostasis.

1. Introduction

As aging populations grow, sight loss is becoming a major world health concern. Eye conditions related to aging share some common pathological characteristics, including the degeneration of the retinal pigment epithelium (RPE) (Ambati et al., 2003) and secondary photoreceptor cell damage (Organisciak and Vaughan, 2010). Several lines of evidence have determined oxidative stress in the RPE to be a major pathogenic element in age-related macular degeneration (AMD) (Shen et al., 2007) and diabetic retinopathy (Du et al., 2013). Oxidative stress refers to elevated intracellular levels of reactive oxygen species (ROS) (Cross et al., 1987), which are produced by damaged mitochondria and which inevitably impair cellular function (Balaban et al., 2005). Recently, oxidative stress was shown to induce an age-dependent increase in ROS levels and cell death in human RPE (He et al., 2014). However, the molecular mechanisms making aging RPE vulnerable to high levels of ROS and subsequent activation of cell death are largely unknown.

We have recently identified the neuroprotective role of prolactin (PRL) in rat retinas (Arnold et al., 2014). PRL is a critical link between the neuroendocrine and immune systems. Notably, deep sequencing experiments showed that increased vulnerability to AMD is due to initially high levels of inflammatory factors and low levels of homeostatic neuroprotective factors, such as the suppressor of cytokine signaling (SOCS) 1 (Mustafi et al., 2012; Swaroop et al., 2009). PRL signaling is down-regulated when SOCS-1 is lost (Minoo et al., 2004). Together, these findings indicate that PRL signaling may play a critical role in the age-related degeneration of the retina.

PRL and its receptor are expressed in the retina (Rivera et al., 2008). Retinas from PRL receptor knockout (*prlr*$^{-/-}$) mice exhibit photoresponsive dysfunction that correlates with reduced rhodopsin levels (Arnold et al., 2014). Given that the RPE normally supplies photopigments to rods (Nandrot et al., 2008), a lack of PRL signaling may alter its function. A previous study demonstrated that most retinal cells are positive for the PRL receptor (Rivera et al., 2008), but whether this receptor is present in the RPE remains to be determined.

In addition, there is abundant evidence of altered Ca^{2+} dynamics in cells with increased age (Toescu et al., 2004) and oxidative stress (Camandola and Mattson, 2011), which are partially mediated by transient receptor potential (TRP) channel dysfunction (Pena and Ordaz, 2008). Notably, TRP melastatin 2 (TRPM2) is a unique Ca^{2+}-permeable,

* Corresponding author at: Instituto de Neurobiología, Universidad Nacional Autónoma de México (UNAM), Campus UNAM-Juriquilla, 76230 Querétaro, Qro., Mexico.
E-mail address: stephaniethebault@gmail.com (S. Thebault).
[1] RMG, DAZ, and EA contributed equally to this work.

http://dx.doi.org/10.1016/j.ebiom.2016.03.048

nonselective cation channel that is responsive to ROS (Faouzi and Penner, 2014) and that has been implicated in cell death in response to oxidative stress (Takahashi et al., 2011). Emerging evidence supports the idea that glutathione (GSH) depletion, which occurs during aging (Rebrin et al., 2007), associates with altered intracellular Ca^{2+} dynamics that may develop in neurons as a result of increased TRPM2-mediated Ca^{2+} influx (Ovey and Naziroglu, 2015). Reinforcing the possibility that TRPM2 may contribute to neurological diseases associated with aging and oxidative stress is the fact that this channel is gated by the sirtuin metabolite 2′O-acetyl-ADP-ribose (Grubisha et al., 2006; Tong and Denu, 2010). Sirtuins are a conserved family of protein/histone deacetylases, of which the founding member Silencing Information Regulator 2 (SIRT2) has been suggested to be neuroprotective when inhibited (Hall et al., 2013). Indeed, reduced *sirt2* expression associates with increased photoreceptor survival in flies (Pallos et al., 2008), although it is not yet clear whether SIRT2 activation has negative effects in aging retinas.

Here we demonstrate that PRL is necessary for the survival of RPE under normal and advancing age conditions. We further identified *SIRT2* and TRPM2 as molecular targets for the antioxidant and anti-apoptotic actions of PRL in the RPE.

2. Materials and Methods

2.1. Reagents

Human recombinant PRL (Freeman et al., 2000) generated in *Escherichia coli* was provided by Michael E. Hodson (Yale University, New Haven, CT). The PRL receptor antagonist Del1-9-G129R-hPRL was produced in *Escherichia coli* and purified as described (Bernichtein et al., 2003). Anti-human PRL rabbit polyclonal antibody IC5 and anti-TRPM2 (#ACC-043) were kind gifts from the National Hormone and Pituitary Program (UCLA Medical School, Torrance, CA) and Alomone Labs, respectively. Normal rabbit serum was collected from control (non-immunized) rabbit whole blood. N-acetyl cysteine (Cat. number A7250) (Mennicke et al., 1987), AGK2 (Cat. number A8231) (Villalba and Alcain, 2012), and piceatannol (Cat. Number P0453) (Gill et al., 1987) were purchased from Sigma-Aldrich (St. Louis, MO). Anti-PRL receptor (U5, Novus Biologicals, Littleton, CO), Alexa-488 goat anti-mouse IgG (ab150117, Abcam, Carlsbad, CA), anti-RPE65 (MAB5528, Chemicon International, Temecula, CA) and anti-β-tubulin (ZYMED from Life Technologies; #22833) antibodies were purchased as specified.

2.2. Ethics Statement

All experiments were approved by the Bioethics Committee of the Institute of Neurobiology from the National Autonomous University of Mexico (UNAM, clave NOM-062-ZOO-1999) in accordance with the rules and regulations of the Society for Neuroscience: Policies on the Use of Animals and Humans in Neuroscience Research. All efforts were made to minimize the number of animals used and their suffering.

2.3. Animal Care and Retinal Tissue

Male albino rats (Wistar, 275 ± 25 g, 7–9 weeks) and 30 male and 30 female albino mice (129Sv, 33 ± 2 g, 3 month old) were fed ad libitum and reared in normal cyclic light conditions (12 h light: 12 h dark) with an ambient light level of approximately 400 lx. Animals were sacrificed by CO_2 inhalation and decapitation. Eyes were enucleated and processed for in situ hybridization and immunohistochemistry.

2.4. Mice

Mice heterozygous for PRL receptor ((Ormandy et al., 1997); 129Sv background) were crossbred, and PRL receptor-null ($prlr^{-/-}$) mice were selected as previously described (Arnold et al., 2014). Wild-type (16 males and 13 females) and $prlr^{-/-}$ (14 males and 17 females) mice were subjected to normal cyclic light until they reach 5 or 14 months of age. After a 24-h dark adaptation period, mice were killed by CO_2 inhalation and decapitation. Eyes were enucleated, and flat mounts of RPE were obtained (Claybon and Bishop, 2011) and processed for histology, apoptosis, and immunostaining, or retinas were obtained for RNA extraction.

2.5. In Situ Hybridization

Sense and antisense PRL receptor RNA probes labeled with digoxygenin were synthesized from a linearized plasmid containing the rat PRL receptor cDNA. Isolated retinas were fixed for 24 h in 4% formaldehyde, incubated for 24 h in RNase-free 10% sucrose-phosphate buffered saline (PBS), then for 3 days in 30% sucrose-PBS. Retinas were embedded in Tissue-Freezing Medium (Leica Instruments, Neussloch, Germany), sectioned (12 μm), and mounted on slides (Superfrost/Plus; A. Daigger & Co., Vernon Hills, IL). Sections were dried for 15 min at 60 °C, fixed with 4% formaldehyde for 10 to 15 min in PBS, and washed in PBT (PBS + 0.1% Tween 20). Sections were incubated in a 1:1 mixture of PBT and hybridization solution (5× sodium chloride and sodium citrate solution), 0.1% Tween 20, 50% deionized formamide, 100 μg/ml sonicated salmon sperm DNA) and prehybridized in hybridization solution for 1 h at 55 °C. Probes were denatured in hybridization solution and allowed to hybridize to tissue sections overnight at 55 °C. Slides were washed at 60 °C with hybridization solution and then with PBT. They were incubated for 2 h with an anti-digoxygenin antibody coupled to alkaline phosphatase (Roche, Basel, Switzerland), then washed in PBT. Signal was detected using tetrazolium blue and 5-bromo-4-chloro-3-indolyl phosphate as substrates in alkaline buffer (Roche).

2.6. Immunohistochemistry

Eyes were fixed in 4% paraformaldehyde. Then, they were either washed overnight in 0.1 M PBS, immersed in 15% sucrose at room temperature, oriented and frozen in Tissue-Tek (Sakura Finetek, Torrance, CA), and sectioned (12 μm thick) along the sagittal axis of the eye or dissected for a whole mount of the RPE as described (Claybon and Bishop, 2011). Retina cryosections and RPE flat mounts were incubated in PBS with 1% SDS for 5 min, rinsed three times with PBS for 5 min, blocked in PBS containing 10% normal goat serum and 0.1% Triton X-100 for 1 h, and then incubated overnight at 4 °C with anti-PRL receptor monoclonal antibody (U5) at 20 μg/ml. The primary antibody reaction was detected using the avidin-biotin complex-detection kit (Vectastain, ABC kit; Vector Laboratories, Burlingame, CA) or labeled with Alexa-488 goat anti-mouse IgG used at 1:200 dilution. RPE flat mounts were then incubated with a 1:1000 dilution of rhodamine phalloidin (R415, Thermo Fisher Scientific, Waltham, MA) for 1 h. Double labeling was performed with both anti-PRL and anti-RPE cell specific antibodies [anti-PRL polyclonal antibody IC5, dilution 1:500; anti-RPE65, at 0.08 μg/ml]. After incubation with the primary antibodies, samples were rinsed 3 times in PBS and labeled for 2 h with Alexa-594-conjugated goat anti-mouse IgG, or Alexa-488-goat anti-rabbit IgG obtained from Molecular Probes (Eugene, OR) and used at dilutions of 1:500 (anti-mouse) or 1:1000 (anti-rabbit), respectively. Control for the U5 anti-PRL receptor antibody was carried out using $prlr^{-/-}$ mice (Fig. 1b), and secondary antibody control for the IC5 anti-PRL antibody was carried out omitting the primary antibody (*data not shown*). Labeled samples were examined with a laser scanning confocal microscope (Zeiss Axiovert 200 LSM 510 Meta, Carl Zeiss International, Oberkochen, Germany). Images were prepared using the Zeiss LSM Image Examiner.

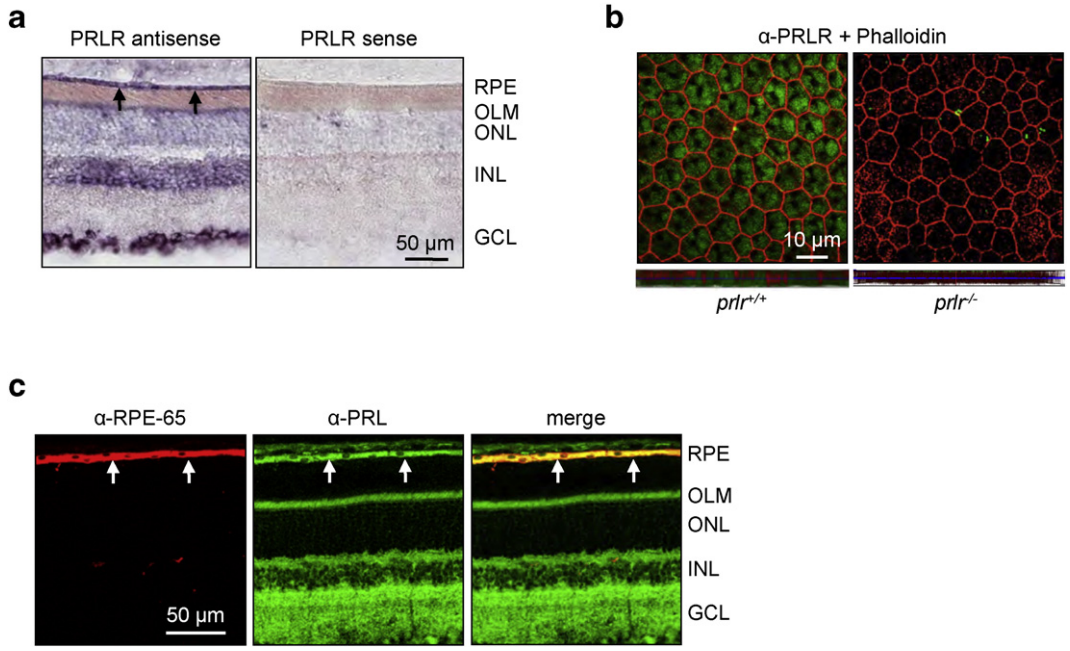

Fig. 1. PRL receptor and PRL expression in the RPE. (a) Representative image of in situ hybridization of transverse sections from rat eyes showed marked expression of the PRL receptor in the RPE, the outer limiting membrane (OLM), the outer (ONL) and inner (INL) nuclear layers, and ganglion cell layer (GCL) with the antisense probe (left panel). No specific staining was observed with the sense probe (right panel). Arrows indicate RPE. (b) Representative confocal stack image of RPE whole mounts from wild-type ($prlr^{+/+}$) and PRL receptor-null ($prlr^{-/-}$) mice showing PRL receptor (green) and F-actin (stained by phalloidin, red) immunofluorescence in x-y axis and z-axis projection (0.5 μm step size). No specific signal against PRL receptor was observed in $prlr^{-/-}$ RPE cells. Corresponding separate x-y axis images were included in Supplemental Fig. 2. (c) Representative confocal images of transverse sections of rat retinas showing RPE-65 (red) and PRL (green) immunofluorescence. PRL was present in choroid and retinal cell layers. Co-labeling of RPE and PRL showed strong immunostaining in the cytoplasm of RPE cells (yellow, right panel). Magnification bars were as indicated. In experiments of each panel, images were captured in three different regions of the same retina section (n = 3). Both retinas of four animals (per group in b) were analyzed (N = 6). Two male and two female from each genotype ($prlr^{+/+}$ and $prlr^{-/-}$) were analyzed in b.

2.7. In Situ Apoptosis

RPE flat mounts were fixed in 4% paraformaldehyde (PFA) and permeabilized with 0.1% Triton X-100 and 0.1% sodium citrate for 7 min followed by incubation in sodium citrate buffer (10 mM sodium citrate, 0.5% Tween 20, pH 6.0) for 1 min at 86 °C. Apoptosis was detected by the terminal deoxynucleotidyl transferase dUTP nick end labeling (TUNEL) method using the In Situ Cell Death Detection Kit (Roche Diagnostics). DNA was stained with DAPI (4′,6-diamidino-2-phenylindole (Stohr et al., 1977), 1 μg/ml, Sigma-Aldrich). Apoptotic signals were visualized under fluorescence microscopy (Microscope BX60F5, Olympus Optical Co. LTD) and quantified by the image analysis system software Pro-Plus (Media Cybernetics Inc.).

2.8. Detection of Intracellular ROS

The in situ production of ROS in the RPE was assessed using dihydroethidium (DHE, structure is provided in Supplemental Fig. 1a) staining. RPE flat mounts were fixed in 4% PFA and mounted on gelatin-coated slides. In a dark chamber, RPE was loaded with 5 μM DHE for 30 min at room temperature and then washed thrice in PBS. RPE was mounted on glass slides with VECTASHIELD® mounting medium with DAPI, and the slides were analyzed without delay using a LSM 510 confocal laser-scanning microscope. Images were obtained using an Apo-406 objective. The same acquisition settings were used for all experiments to allow direct comparison of RPE flat mounts. Digital images were processed using free ImageJ software (V.1.36, National Institutes of Health). Only cropping of images was performed; there was no adjustment of brightness. The mean fluorescence intensity ratio in RPE was determined in 6 different regions of interest (same size), distributed equally over the full layer, from three flat mounts per condition. The ratio between DHE (numerator) and DAPI was calculated to determine superoxide anion production in the three experimental groups.

2.9. Cell Culture

The ARPE-19 human cell line was purchased from ATCC (Number: CRL-2302) (Dunn et al., 1996) and was grown in Dulbecco's Modified Eagle's Medium nutrient mixture F12 supplemented with 10% fetal bovine serum and 1% penicillin/streptomycin. Cultures were seeded at an initial density of 10^6 cells and maintained at 37 °C and 5% CO_2. Because serum contains variable mixtures of factors that might modulate the effects of PRL, we preincubated the cultures in serum-reduced (1%) medium for 12 h prior treatments.

2.10. RNA Isolation and cDNA Synthesis

Retinas were dissected for mRNA analysis. Total RNA from retinas and ARPE-19 cells was isolated using TRIzol reagent (Invitrogen, Waltham, MA). Total RNA was quantified. For retina RNA, contaminating genomic DNA was removed using 1 ml of RNase-free DNase I (BoehringerMannheim)/10 mg of RNA at 37 °C for 30 min. A 1-mg sample (retinas) and a 2-μg sample (ARPE-19 cells) were reverse-transcribed using the High-Capacity cDNA Reverse Transcription Kit (Life Technologies, Carlsbad, CA).

2.11. Conventional PCR

For the PCR reaction, specific sense and antisense primers were selected (Table 1), based on GenBank TRP sequences, using GeneJockey II (Biosoft, Cambridge, UK). Each sample was amplified using Maxima SYBR Green/ROX qPCR Master Mix (Thermo Scientific, Auburn, AL) in an automated thermal cycler (Bio-Rad CFX96 Real-Time System; Bio-Rad Laboratories, Hercules, CA). DNA amplification conditions included

an initial 7-min denaturation step at 95 °C (which also activated the AmpliTaq Gold) and 40 cycles of 30 s at 95 °C; 30 s at 57 °C for the PRL receptor, 60 °C for TRPM2, and 57 °C for glyceraldehyde-3-phosphate dehydrogenase (GAPDH); 40 s at 72 °C, and a final elongation of 7 min at 72 °C. The RT-PCR samples were electrophoresed on a 1.5% agarose gel and stained with ethidium bromide (0.5 μg/ml), then photographed under UV light.

2.12. Quantitative PCR

PCR products were detected and quantified with Maxima SYBR Green qPCR Master Mix (Thermo Scientific) in a 10-μl final reaction volume containing template and 0.5 μM of each of the primer pairs (Table 2). Amplification performed in the CFX96 real-time PCR detection system (Bio-Rad, Hercules, CA) included a denaturation step of 10 min at 95 °C, followed by 40 cycles of amplification (10 s at 95 °C, 30 s at the primer pair–specific annealing temperature, and 30 s at 72 °C). The PCR data were analyzed by the 2–ΔΔCT method, and cycle thresholds normalized to the housekeeping gene TBP were used to calculate the mRNA levels of interest.

2.13. Transient Transfection

ARPE-19 cells were transfected with 50 nM siRNA against human TRPM2 (SMARTpool: SiGENOME TRPM2 siRNA, NCBI substance Id 152147430, GE Dharmacon, Lafayette, CO) using Lipofectamine 2000 (Invitrogen). Control experiments were performed by transfecting the SiGENOME non-targeting control siRNAs, Cat# D-001210-01-05, GE Dharmacon) or by exposing cells to Lipofectamine 2000 without siRNA. Analysis of protein content, Ca^{2+} imaging and survival assays were performed 24 h after transfection.

2.14. Immunocytochemistry

ARPE-19 cell cultures were fixed in 4% PFA for 1 h, incubated in PBS with 1% SDS for 5 min, rinsed three times with PBS for 5 min, blocked in PBS containing 10% normal goat serum and 0.1% Triton X-100 for 1 h, and then labeled overnight at 4 °C with anti-PRL receptor monoclonal antibody (U5) at 20 μg/ml. The primary antibody was detected with Alexa-488 goat anti-mouse IgG (ab150117) used at 1:200 dilution. F-actin was stained with a 1:1000 dilution of rhodamine-phalloidin (R415, Thermo Fisher Scientific, Waltham, MA, structure is provided in Supplemental Fig. 1b) for 1 h. Samples were then mounted on glass slides with VECTASHIELD® mounting medium with DAPI. Labeled samples were examined with a laser scanning confocal microscope (Zeiss Axiovert 200 LSM 510 Meta). Images were prepared using the Zeiss LSM Image Examiner.

2.15. Immunoblotting

Conditioned media from 3-day confluent ARPE-19 cell cultures were collected and concentrated 30-fold using Amicon® Ultra centrifugal filters (Merck Millipore, Darmstadt, Germany). In another group of experiments, ARPE-19 cells were transfected with siRNA against human TRPM2 or control siRNA for 48 h. Protein samples were resuspended in lysis buffer (0.5% Igepal, 0.1% SDS, 50 mM Tris, 150 mM NaCl, 1 μg/ml aprotinin, and 100 μg/ml PMSF, pH 7.0), and subjected to SDS/PAGE; total protein (40 μg) was blotted and probed overnight with a 1:500 dilution of anti-PRL IC5 antibody, a 1:200 dilution of anti-TRPM2 or a 1:1000 dilution of anti-β-tubulin antibodies. Primary antibody detection was performed using an alkaline phosphatase-coupled secondary antibody and a colorimetric detection kit (Bio-Rad).

2.16. Viability Assay

The reduction of 3-(4,5-dimethylthiazolyl-2)-2,5-diphenyltetrazolium bromide (MTT) was used as an index of RPE cell survival. Cells were seeded in 96-well collagen-coated flat bottom microculture plates (Corning) at an initial density of 2500 cells/well and treated for 48 h with 1% FBS culture medium supplemented or not (control) with 100 pM PRL, anti-human PRL antibody (dilution 1:500; defined in pilot experiments), normal serum control, Del1-9-G129R-hPRL (0.1 and 1 μM; defined in pilot experiments), or increasing doses of H_2O_2, as indicated. In another group of experiments, ARPE-19 cells were incubated with 100 μM H_2O_2 in the presence or absence of 100 pM PRL, 10 μM antioxidant N-acetyl cysteine, 10 μM SIRT2 inhibitor AGK2 or siRNA against TRPM2, as indicated. Piceatannol (10 μM) was also tested. The dose of hPRL (100 pM) that maximally promoted ARPE-19 cell survival was determined by performing a dose-response assay (not shown). Based on PRL levels detected in 10% FBS medium (Fig. 2e), we calculated that 1% FBS medium contains a few pg/ml of PRL, which may be considered negligible compared to the concentrations present in the conditioned medium of ARPE-19 cells (1.7 ± 2.1 ng/ml, Fig. 2e) and the 100 pM (i.e. 2.3 ng/ml) exogenously administered PRL. Next, cells were incubated with MTT (500 mg/ml, Sigma-Aldrich) at 37 °C for 3 h, and the formazan precipitate was solubilized with 0.4 N HCl containing 10% SDS for 30 min at room temperature and quantified by measuring absorbance at 570 nm.

2.17. Cell Proliferation Assay

Cell proliferation was assessed by [3H]thymidine incorporation (Amersham International plc, Cardiff, UK). The [^{3}H]thymidine incorporation assay consisted in seeding cells in 48-well collagen-coated flat-bottom microculture plates (Corning) at an initial density of 5000 cells/well and subjecting them to a series of treatments (all in 200 μl of culture medium containing 1% FBS) that included a 24-h incubation with recombinant human PRL (100 pM) combined or not with Del1-9-G129R-hPRL (1 μM), or with H_2O_2 (100 μM). Twenty-four hours before ending the treatment, 1 μL of [^{3}H]-thymidine per well was added. After the 48-h treatment, wells were washed thrice in 5% trichloroacetic acid, with the last wash for 20 min at 4 °C. Next, 250 μL boiling 0.25 N NaOH was added, and samples were transferred to scintillation vials for quantification.

2.18. Apoptosis Detection

ARPE-19 cells were assayed for apoptosis by measuring fragmented nucleosomal DNA using the Cell Death Detection ELISA Kit (Roche).

2.19. Measurement of Total ROS and Antioxidant Capacity Using the Victor^3 V Microplate Reader

Total ROS levels (The Enzo Life Sciences' Total ROS/Superoxide detection kit; ENZ-51010) and antioxidant capacity (Cayman Chemical, Ann Arbor, MI; 709001) were assessed according to the Manufacturer's instructions.

2.20. Quantification of GSH Levels

GSH levels in lysates from ARPE-19 cells were measured with the GSH-glo-glutathione-assay (Promega) according to the Manufacturer's instructions. GSH concentrations were determined by interpolation from a GSH standard curve generated using the bioluminescent system.

2.21. Ca^{2+} Imaging

For Ca^{2+} imaging studies, ARPE-19 cells at confluence were plated onto round coverslips covered with poly-L-lysine (10 μg/ml, Sigma

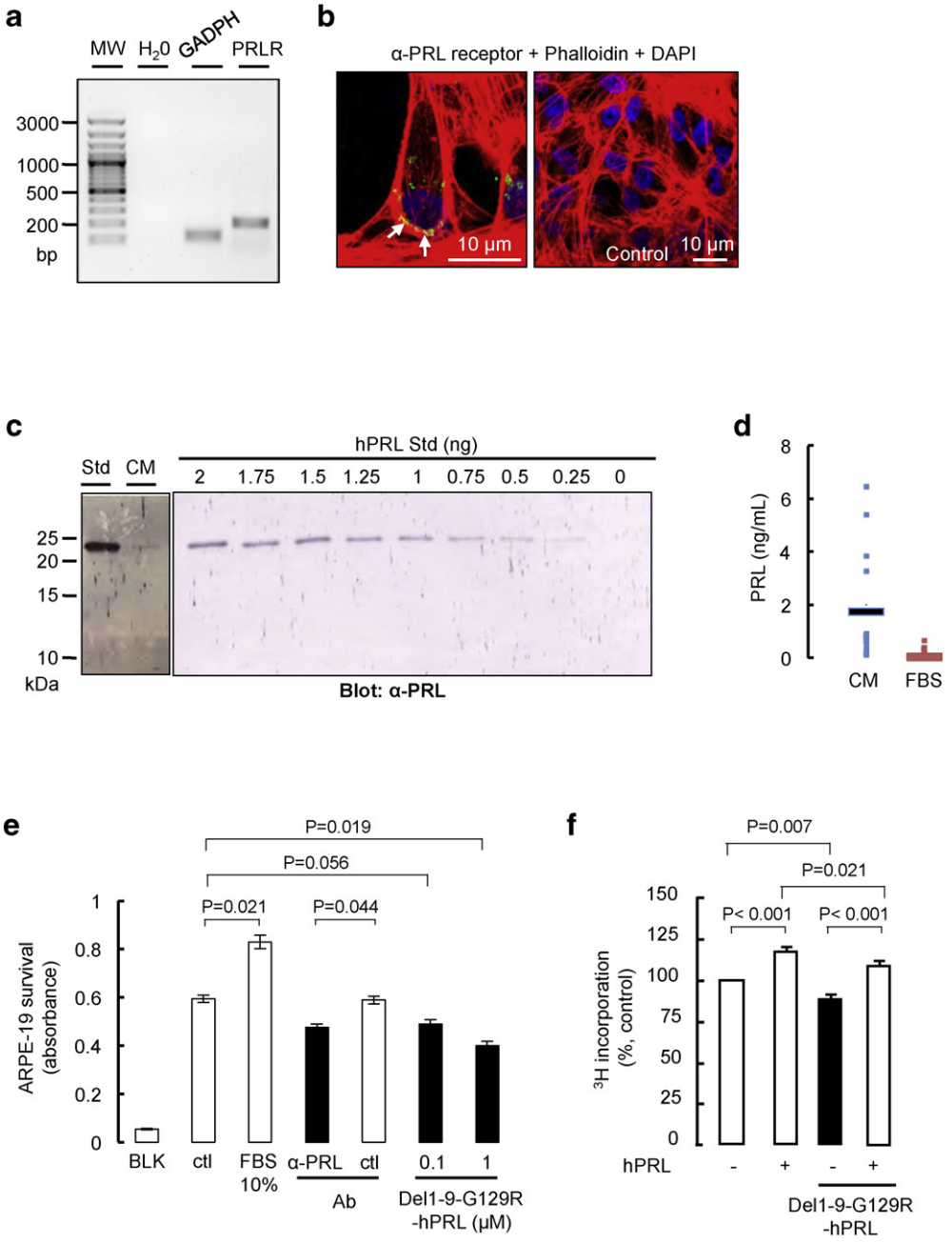

Fig. 2. Endogenous PRL is a trophic factor for RPE cells. (a) RT-PCR of PRL receptor (PRLR, 200 bp) in ARPE-19 cell extracts. GAPDH was used as a positive control. bp, DNA ladder. RT-PCR was performed in RNA extracted from three independent cell cultures (N = 3). (b) Confocal stack image of ARPE-19 cells showing F-actin (red), nucleus (blue), and PRL receptor (green) immunofluorescence in x-y axis. Corresponding x-y axis images and z-axis projection were included in Supplemental Fig. 3a and b, respectively. PRL receptor was present in a non-uniform, punctuate distribution along the ARPE-19 cell border (left panel). The secondary antibody control was carried out by omitting the anti-PRL receptor antibody (right panel). Images were captured in three different regions of the culture plate (n = 3), three independent cultures were analyzed (N = 3). (c) Western blot analysis of PRL in conditioned media (CM) from 3-day ARPE-19 cells. A standard of 23-kDa PRL (Std) was included, and equal concentrations of total proteins were loaded. Also, a series of standard PRL dilutions was included at indicated concentrations. CM from five 3-day ARPE-19 cell cultures concentrated by a ~2-fold factor was analyzed and this same experiment was repeated three times (N = 3). (d) Quantification of PRL in the CM of 3-day ARPE-19 cells by the Nb2-bioassay. 10% FBS medium was included. Note that CM was not concentrated. Three samples from CM from five 3-day ARPE-19 cell cultures were analyzed and this same experiment was repeated three times (N = 3). (e) Effect on survival of ARPE-19 cells treated with 10% FBS, polyclonal α-PRL antibody (α-PRL Ab) or preimmune serum (ctl Ab), pure PRL receptor antagonist Del1-9-G129R-hPRL at 0.1 and 1 μM or untreated (ctl) for 48 h was measured by MTT assay (n = 8; N = 3 independent experiments). BLK, averaged blank. (f) ARPE-19 proliferation after treatment with 100 pM hPRL, 1 μM Del1-9-G129R-hPRL or no treatment was measured by incorporation of [^{3}H]thymidine for 24 h after the treatments. Scintillation signals were normalized to the untreated condition (n = 9; N = 3 independent replicates). All bar plots, mean plus S.E.M.; *P* values: ANOVA and Bonferroni *post-hoc* test. Of note, the control condition corresponds to cells that were pre-treated with 1% FBS medium during 12 h followed by a 48-h period in the same medium.

Chemical) and incubated in the dark with 10 μM fluo 8-AM (Invitrogen) dissolved in the extracellular buffer containing: 150 mM NaCl, 20 mM HEPES, 0.1 mg/ml bovine serum albumin, 1.0 mM EGTA, adjusted to pH 7.4 with NaOH. Loaded cells were transferred into a perfusion chamber located on a microscope adapted to an epifluorescence system (Eclipse E600FN; Nikon Melville, NY). Cells were constantly perfused with oxygenated extracellular buffer at a rate of 15–17 ml/min and at 29–30 °C. Excitation of the fluorophore (at 488 nm) was performed with a light source controlled by a Lambda LS illuminator (Sutter Instruments, Novato, CA). Images were acquired with a cooled digital camera

(Cool-SNAP-ES, Roper Scientific, Tucson, AZ) using the RS image software (Photometrics; Roper Scientific). The image field was 800 × 600 μm in size (Ramirez et al., 2012). Short movies (180 s total time, at 40 ms exposure at 4 Hz) were taken in control conditions and during the wash-in of the pharmacological treatments. To normalize the change in fluorescence of the treated cultures, their Δ fluorescence was corrected by subtracting that of one of the untreated conditions.

2.22. Image Analysis

Images were analyzed using Image J (V.1.36, National Institutes of Health). The cells in a field were semiautomatically identified, and their mean fluorescence was measured as a function of time. Single-pixel noise was removed using a 5-pixel ratio mean filter. Ca^{2+}-dependent changes in fluorescence (Δ fluorescence) were computed as $(F_i - F_o) / F_o$ where F_i is fluorescence intensity at any given frame, and F_o is the resting fluorescence.

2.23. Statistical Analysis

In general, all results were replicated in three or more independent experiments. The number of replicates (n) in each experiment and how often it was independently repeated (N) is indicated in each figure legend. Serum PRL levels are reported as mean ± S.D. and all others as mean ± S.E.M.; all data showed normal distribution or equal variance according to D'Agostino-Pearson omnibus and Levene's tests, respectively. Statistical differences between two groups were determined by a two-tailed Student's *t*-test, among three groups with one variable by one-way ANOVA followed by Bonferroni's *post-hoc* comparison test, and among four groups with two variables by two-way ANOVA followed by Bonferroni's *post-hoc* comparison test (Sigma Stat 7.0, Systat Software Inc., San Jose, CA). Differences in means with $P < 0.05$ were considered statistically significant.

2.24. Gender Analysis

Mice of both genders (ratio almost 1:1 for wild-type: 16 males and 13 females, and $prlr^{-/-}$ mice: 14 males and 17 females) were used. We did not assess the stage of estrous. Independent analysis for either sex did not show any significant difference in the PRL receptor distribution or in the assays presented in Fig. 6 (data not shown).

3. Results

3.1. PRL and PRL Receptor are Present in Rodent RPE

PRL receptor mRNA was found in the RPE layer from rat retinal cross sections by in situ hybridization (Fig. 1a). Immunohistochemistry using the U5 anti-PRL receptor antibody labels the PRL receptor in whole mounts of mouse RPE, whereas no specific signal appeared in $prlr^{-/-}$ RPE (Fig. 1b).

PRL signaling is triggered by PRL binding to preformed PRL receptor homodimers (Tallet et al., 2011). Immunohistochemistry was performed on retina sections using RPE-65 isomerase as an RPE marker (Hamel et al., 1993). We observed immunopositive staining for PRL in RPE-65-expressing cells (Fig. 1d). PRL colocalized with RPE-65 within the cytoplasm of RPE cells.

All together, these data suggest that the RPE is a target for autocrine/paracrine actions of PRL.

3.2. Endogenous PRL is a Trophic Factor for Human RPE cells

To explore the direct effects of the PRL signaling pathway on the RPE, we first used a human RPE cell line, ARPE-19 (Dunn et al., 1996), in which we found both PRL receptor mRNA (Fig. 2a) and protein (Fig. 2b). We also observed that PRL was present in the conditioned medium of ARPE-19 cell cultures (Fig. 2c). We assessed levels of bioactive PRL using the Nb2-cell bioassay and found a PRL concentration of 1.7 ± 2.1 ng/ml in the conditioned medium of ARPE-19 cell cultures (Fig. 2d). Of note, 10% FBS medium contained 0.031 ± 0.18 ng/mL (Fig. 2d). Previous studies demonstrated that PRL regulates cell survival, proliferation, and apoptosis in a variety of cell types (Adan et al., 2013; Morales, 2011; Yu-Lee, 2002). To assess the direct involvement of endogenous PRL in RPE cell survival, ARPE-19 viability was tested in the presence of anti-PRL polyclonal antibody (Castilla et al., 2010), normal rabbit serum or the competitive PRL receptor antagonist Del1-9-G129R-hPRL (Bernichtein et al., 2003) for 48 h. Both anti-PRL antibody and the highest dose of Del1-9-G129R-hPRL decreased ARPE-19 cell survival by 20–30% relative to the control, while pre-immune serum did not (Fig. 2e). Using ^{3}[H] incorporation, we showed that Del1-9-G129R-hPRL diminished ARPE-19 cell proliferation by 13 ± 3% and also prevented the proliferative effect of recombinant human PRL (hPRL, Fig. 2f).

3.3. PRL Protects and Rescues Human RPE Cells From Hydrogen Peroxide (H_2O_2)-induced Damage

The RPE is in a location in the retina where it is in constant contact with ROS. H_2O_2 has been used as a direct oxidant to initiate and study cellular oxidative stress, because it is generated by the RPE during phagocytosis of the photoreceptor outer segments (Miceli et al., 1994). Dose-response experiments showed that H_2O_2 markedly inhibited ARPE-19 cell survival with an IC_{50} of 57 μM after a 24-h treatment (Fig. 3a). Using 100 μM H_2O_2, we showed that this effect involved both a drastic reduction of cell proliferation (82 ± 6%; Fig. 3b) and a marked increase in apoptosis (51 ± 12%; Fig. 3c), as determined by internucleosomal DNA fragmentation measured by ELISA. We next evaluated whether PRL protected against the effect of a 24-h exposure to 100 μM H_2O_2 (Fig. 3d). H_2O_2 reduced RPE cell survival (Fig. 3e) and induced apoptosis (Fig. 3f), and these effects were prevented by PRL. Alone, PRL promoted the survival of ARPE-19 cells, but it did not modify their levels of apoptosis. We then investigated restorative properties of PRL by administering PRL 18 h after H_2O_2 treatment (Fig. 3g), i.e., when oxidative damage is evident (Fig. 3h, i). PRL reversed the reduction in cell survival (Fig. 3h) and the increase in apoptosis (Fig. 3i) induced by H_2O_2. Alone, PRL did not modify ARPE-19 cell survival or apoptosis.

3.4. PRL Reduces Intracellular Levels of ROS in Human RPE Cells, Thus Decreasing the Cytotoxic Effect of SIRT2

Serum levels of PRL were previously shown to positively correlate with superoxide dismutase (SOD) activity in mammary tissues (Bolzan et al., 1995), but whether PRL directly favors an antioxidant environment remains elusive. The antioxidant N-acetyl cysteine (Kerksick and Willoughby, 2005) prevented the reduction in ARPE-19 cell survival induced by H_2O_2 (Fig. 4a), thereby mimicking PRL actions. Further, PRL reduced the increase in total ROS levels associated with H_2O_2 exposure to control levels (Fig. 4b). Alone, PRL decreased the total levels of ROS. We showed that ARPE-19 cells increased their antioxidant capacity by 1.8-fold in response to H_2O_2, and by 3.6-fold in the presence of PRL and H_2O_2 (Fig. 4c), but PRL alone did not modify the antioxidant capacity. The mRNA levels of endogenous antioxidant enzymes such as catalase, SOD, and glutathione peroxidase were assessed by quantitative PCR. Fig. 4d shows that exposure to H_2O_2 increased the levels of Mn^{2+}-SOD, Cu^{2+}-SOD, and glutathione peroxidase mRNA by 45 ± 1.0%, 30 ± 0.5%, and 36 ± 0.5% of controls, respectively, but did not alter catalase levels. PRL did not modify the H_2O_2-mediated increase in Mn^{2+}-SOD, Cu^{2+}/Zn^{2+}-SOD, and glutathione peroxidase levels, nor did PRL change catalase mRNA levels. PRL by itself did not modify the mRNA levels of any of these enzymes. Additionally, we quantified reduced GSH levels since N-acetyl cysteine, which mimics PRL actions, is a precursor of glutathione.

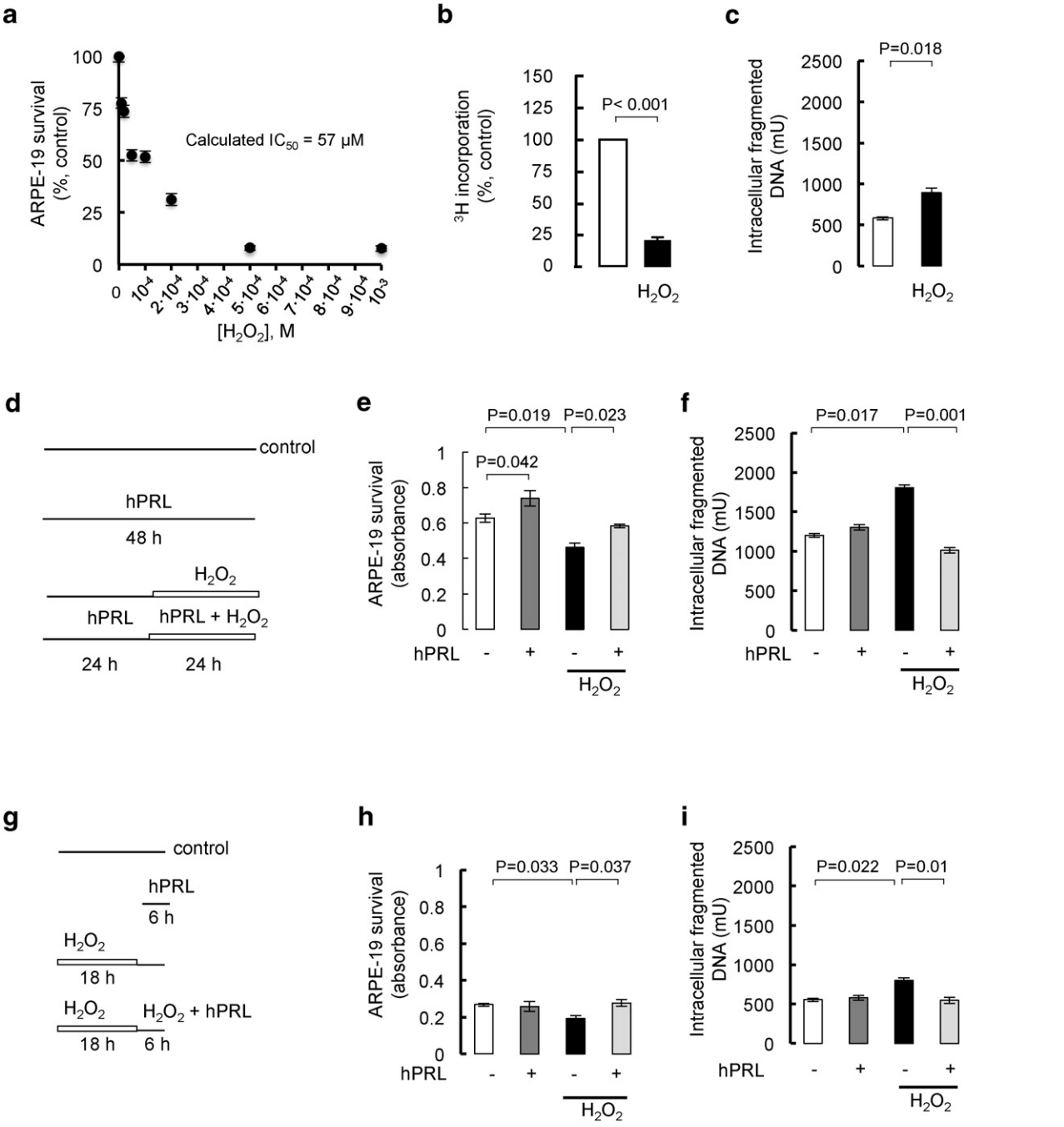

Fig. 3. PRL promotes human RPE cell survival. (a) Dose-response curve showing the inhibitory effect of hydrogen peroxide (H_2O_2) on ARPE-19 survival. Increasing H_2O_2 doses diminished ARPE-19 cell survival. (b) Proliferation of ARPE-19 cells was reduced by 82 ± 6% and (c) apoptosis was increased by 51 ± 12% with 100 μM H_2O_2 present for 24 h. (d) Timeline diagram depicting the design of the preventive experiments e and f. (e) When applied alone, hPRL promoted ARPE-19 cell survival, while application of hPRL 24 h before the 24-h treatment with 100 μM of H_2O_2, prevented the H_2O_2-induced reduction of survival. (f) hPRL prevented the H_2O_2-mediated increase of apoptosis, while it had no effect alone. (g) Timeline diagram depicting the design of the restorative experiments h and i. (h, i) When applied during the last 6 h of a 24-h treatment with 100 μM H_2O_2, hPRL prevented the H_2O_2-induced reduction of survival (h) and the H_2O_2-mediated induction of apoptosis (i), while hPRL alone had no effect. Note that the restorative scheme of hPRL administration showed results similar to those with the preventive scheme of administration. Incorporation of [^{3}H]thymidine was normalized to the untreated condition. ($n = 12$; $N = 3$ independent replicates). All bar plots, mean plus S.E.M.; *P* values: ANOVA and Bonferroni *post-hoc* test. Of note, the control condition corresponds to cells that were pre-treated with 1% FBS medium during 12 h followed by a 24-h (b, c, h, and i) or 48-h (e, f) period in the same medium.

Exposure to H_2O_2 almost totally eliminated GSH, an effect that was not only prevented but also reversed by PRL (Fig. 4e). Alone, PRL did not modify GSH levels. These results indicate that PRL limits the impact of oxidative stress in human RPE.

H_2O_2 has been found to induce expression of the deacetylase SIRT2 in prostate epithelial cells (Nie et al., 2014), and PRL receptor dimerization and subsequent signaling are inhibited by SIRT2-mediated deacetylation (Ma et al., 2010). SIRT2 is expressed in the retina (Geng et al., 2011), and SIRT2 inhibitors, including AGK2, can decrease cell death in various models of neurodegeneration (Villalba and Alcain, 2012). qPCR analysis of the *SIRT2* gene showed that PRL prevented the 2.4-fold increase in SIRT2 mRNA levels induced by H_2O_2 compared with levels in untreated conditions (Fig. 4f). Alone, PRL did not modify the ARPE-19 cell content of SIRT2 transcript. We also found that

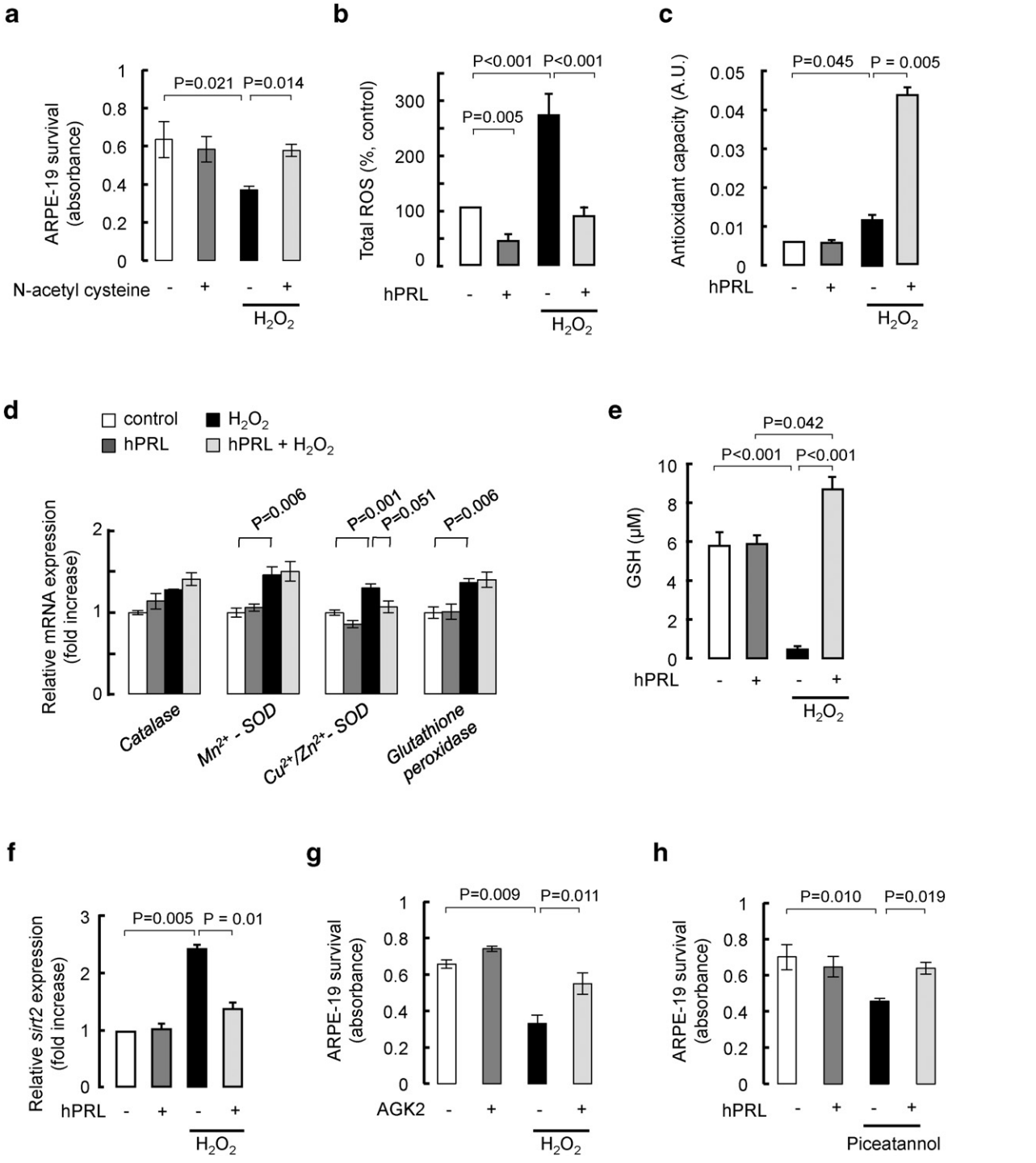

Fig. 4. PRL boosts antioxidant defenses and prevents the oxidant-induced SIRT2 effects on human RPE cells. (a) Effect of the antioxidant N-acetyl cysteine (NAC, 10 mM) on ARPE-19 survival. NAC was applied 24 h before of the 24-h H_2O_2 insult. (b) ROS production and (c) antioxidant capacity in control condition, following H_2O_2 (100 μM) treatment for 24 h, and in the presence of hPRL (100 pM) for 48 h alone or 24 h before the 24-h treatment with H_2O_2. The same treatment scheme was used in d, e, and f. (d) qRT-PCR analyses of mRNAs for catalase, Mn^{2+}-dependent SOD (Mn^{2+}-SOD), Cu^{2+}/Zn^{2+}-dependent SOD (Cu^{2+}/Zn^{2+}-SOD), and glutathione peroxidase in ARPE-19 cell lysates. qRT-PCR data are normalized to TBP levels ($n = 3$; $N = 3$ independent replicates). (e) Reduced glutathione (GSH) levels in lysates from ARPE-19 cells. (f) qRT-PCR analyses of SIRT2 mRNA in ARPE-19 cells. qRT-PCR data were normalized to TBP levels ($n = 3$–6; $N = 3$ independent replicates). (g) Effect of the SIRT2 inhibitor AGK2 on ARPE-19 survival. AGK2 (10 μM) was applied 24 h before of the 24-h H_2O_2 insult. (h) Effect of hPRL on ARPE-19 survival challenged by the SIRT2 activator piceatannol. When hPRL (100 pM) was applied 24 h before of the 24-h piceatannol (10 μM) challenge, it prevented piceatannol-induced reduction of survival. ROS accumulation values were normalized to the untreated conditions. Excluding (d), $n = 12$; $N = 3$ independent replicates. All bar plots, mean plus S.E.M.; *P* values: ANOVA and Bonferroni *post-hoc* test. Of note, the control condition corresponds to cells that were pre-treated with 1% FBS medium during 12 h followed by a 48-h period in the same medium.

treatment with AGK2 opposed the reduction in ARPE-19 cell survival induced by H_2O_2 (Fig. 4g), as did PRL. Alone, AGK2 did not modify ARPE-19 cell survival. To test the possibility that PRL preserves the integrity of human RPE by inhibiting SIRT2, we used piceatannol, an analog of resveratrol (Piotrowska et al., 2012) known to stimulate SIRT2 (Howitz et al., 2003). Like H_2O_2, piceatannol (10 μM, (Piotrowska et al., 2012)) diminished ARPE-19 cell survival, an effect that was blocked by PRL (Fig. 4h).

3.5. PRL Maintains Human RPE Cell Survival by Inhibiting the Oxidant-induced SIRT2-dependent Increase in Intracellular Ca^{2+} That is Mediated by TRPM2 Channels

Previous studies demonstrated that SIRT2 activity produces 2′O-acetyl-ADP-ribose (Zheng, 2013), a metabolite that binds the cytosolic, C-terminus of TRPM2 channels, leading to an increase in intracellular Ca^{2+} levels that correlates with cell death (Faouzi and Penner, 2014). While TRPM2 mRNA has been reported in the retina (Gilliam and Wensel, 2011), the presence of these channels in RPE is unknown. We found that ARPE-19 cells expressed TRPM2 mRNA (Fig. 5a) and protein (Fig. 5b). siRNA against TRPM2 decreased protein levels of the channel in ARPE-19 cells (Fig. 5b). Using the Ca^{2+} indicator fluo-8, we observed that exposure to H_2O_2 elicited a sustained increase in intracellular Ca^{2+} levels that was prevented by siRNA against TRPM2 or by a 15-min pretreatment with PRL (Fig. 5c). Scrambled siRNA or PRL alone did not modify intracellular Ca^{2+} levels. We observed that SIRT2 activation by piceatannol caused an increase in intracellular Ca^{2+} levels that had similar amplitude and kinetics to the one evoked by H_2O_2, and that was inhibited by siRNA against TRPM2 or PRL (Fig. 5d). We also found that the H_2O_2-mediated increase in intracellular Ca^{2+} levels was prevented by a 15-min pretreatment with AGK2 (Fig. 5e). We then evaluated whether the inhibition of TRPM2 channels preserved human RPE survival under oxidant conditions. We found that siRNA against TRPM2 minimized the reduction in ARPE-19 cell survival induced by H_2O_2 (Fig. 5f). Scrambled siRNA did not modify the levels of ARPE-19 survival in the presence of H_2O_2.

3.6. RPE Degeneration is Enhanced During Advancing Age and in Mice Lacking PRL Receptor

In order to examine the *in vivo* relevance of our findings, whole mounts of RPE from 5- and 14-month-old $prlr^{-/-}$ mice were evaluated by the TUNEL assay. In young mice, there was positive TUNEL signal in the RPE (Fig. 6a), indicating that PRL is required for the survival of RPE under normal conditions. Apparent morphological alterations including an increased number of cells that have more than two nuclei were also detected in the 5-month-old $prlr^{-/-}$ mice. Consistent with RPE degeneration being a feature of age-related retinal degeneration (Nag and Wadhwa, 2012), 14-month-old $prlr^{+/+}$ mice showed more TUNEL signal in RPE, compared to that in 5-month-old $prlr^{+/+}$ mice (Fig. 6a). Positive TUNEL signal was also present in the RPE from $prlr^{-/-}$ mice with advancing age (Fig. 6a). The higher levels of apoptosis in 5- and 14-month-old $prlr^{-/-}$ RPE were statistically significant after quantifying the TUNEL signal (Fig. 6b). Also, the number of RPE cells decreased in 5-month-old $prlr^{-/-}$ mice compared with age-matched wild-type counterparts, and they had more nuclei (Fig. 6b). Evaluation of the surface and perimeter of individual RPE cells showed hypertrophy of RPE cells from $prlr^{-/-}$ mice compared with those from wild-type counterparts: RPE cell surface and perimeter were higher in 5- and 14-month-old $prlr^{-/-}$ mice compared with age-matched wild-type mice, respectively (Fig. 6c). However, the surface and perimeter of RPE cells from 5-month-old wild-type and $prlr^{-/-}$ mice were similar to those of 14-month-old wild-type and $prlr^{-/-}$ mice, respectively (Fig. 6c). These data suggest that PRL helps to maintain the morphology of RPE, and that this effect was independent of age. We then analyzed the production of superoxide anion in whole mounts of RPE. Fig. 6d shows representative images of whole mounts of RPE stained with the oxidative fluorescent dye dihydroethidium (DHE), and quantification using the mean pixel fluorescence intensity ratio of DHE/DAPI is provided in Fig. 6e. The RPE from young $prlr^{-/-}$ mice produced more superoxide anion than RPE from age-matched wild-type counterparts. While superoxide anion levels were higher in the RPE from 14-month old $prlr^{+/+}$ mice than those of young mice, they were similar in the RPE of 14-month old $prlr^{+/+}$ and $prlr^{-/-}$ mice. We then explored whether reduced overall synthesis of antioxidant enzymes correlates with increased oxidative stress in $prlr^{-/-}$ retinas. Catalase mRNA levels were reduced in young $prlr^{-/-}$ retinas by 55 ± 3% compared with values from age-matched $prlr^{+/+}$ retinas (Fig. 6f). Consistent with oxidative stress being a hallmark of aging retina (Ardeljan and Chan, 2013), catalase expression was reduced equally in retinas of $prlr^{+/+}$ and $prlr^{-/-}$ mice with advancing age. Lack of PRL receptor or advancing age *per se* was accompanied by a 2.4- or 3.5-fold increased synthesis of SIRT2 in the retina, respectively, compared to young wild-type retinas (Fig. 6f). The SIRT2 mRNA levels were comparable in the retinas of 14-month old $prlr^{+/+}$ and $prlr^{-/-}$ mice. Further, we measured negligible levels of PRL receptor and PRL mRNA in the retina of 14-month old mice (Fig. 6g), supporting the notion that under the oxidative conditions accompanying aging, increased levels of SIRT2 are associated with reduced PRL signaling and RPE cell death.

4. Discussion

The multigenic and complex etiology of age-related retinal diseases in humans is responsible for the relative paucity of effective compounds for their early prevention and treatment. Given that the relationship between the RPE and photoreceptors is crucial to sight (Sparrow et al., 2010), identifying pathways necessary for RPE function is essential to uncover therapies for blindness. The present study identifies the PRL signaling pathway in the adult RPE and demonstrates that it is necessary for RPE survival. PRL receptor antagonism or deficiency increases RPE apoptosis both *in vitro* and *in vivo* and conversely, PRL receptor stimulation promotes the resistance of RPE cells to oxidative stress. One of the mechanisms by which PRL signaling mediates its protective effects in the RPE is through antioxidant actions that lead to decreased SIRT2 expression and TRPM2 inhibition. This study strengthens the significance of the PRL pathway beyond its classical roles in lactation since no sex-based difference in PRL-mediated RPE effects were observed in our experimental conditions. Nevertheless, it is possible that sex-based differences do occur under physiological conditions such as pregnancy and lactation given that the amplitude of the ERG B-wave is higher in pregnant women (De Luca Brunori et al., 1985).

Although the role of PRL in NO signaling has been widely studied (Duckles and Miller, 2010), the direct action of PRL on ROS has not been shown previously. In response to oxidative stress, we found that PRL reduced the levels of ROS and promoted the antioxidant capacity of ARPE-19 cells by increasing GSH levels in the RPE. More importantly, $prlr^{-/-}$ RPE exhibited increased staining for the superoxide indicator DHE, and mRNA levels of catalase were reduced in $prlr^{-/-}$ retinas originating from young or aging mice. These data are consistent with the observations that reduced levels of circulating PRL associate with increased plasma oxidant status in rats (Yuksel et al., 2015). However, blockage of PRL secretion was also reported to associate with enhanced antioxidant defense (Ricke-Hoch et al., 2014) and more particularly, with increased activity of antioxidant enzymes like catalase (Brown-Borg et al., 1999). The reasons for this inconsistency are unknown but may relate to the finely tuned balance between ROS levels and antioxidant defenses. It is clear that if ROS levels are high enough to overwhelm the antioxidant defenses or if the antioxidant protective mechanisms are compromised, then the resulting oxidative stress may lead to aberrant cell signaling through oxidative modification of redox-sensitive signaling proteins (Finkel and Holbrook, 2000). Whether PRL or its receptor are susceptible to oxidative modifications remains to be investigated. The present study also shows that advancing age associates with decreased expression of PRL and PRL receptor in the retina. Whether the down-regulation of PRL and its receptor occurs specifically in the RPE was not determined. Nonetheless, increased oxidative stress and phenotypic changes in the RPE have been reported (Zhao et al., 2011). Along this line, the best-validated therapies remain oral antioxidant supplements based on those investigated in the Age-Related Eye Disease Study (AREDS) and the recently completed AREDS 2 (Broadhead et al., 2015; Wei et al., 2016). Here, we show that N-acetyl cysteine

which, like PRL, allows more GSH to be produced, preserves the integrity of ARPE-19 cells under oxidative stress. Moreover, we found that PRL *per se* reduced intracellular levels of ROS without modifying the antioxidant capacity of ARPE-19 cells. The mechanism underlying this effect has not been explored, but the expression of PRL receptors positively correlates with mRNA abundance for uncoupling proteins UCP1 (Bispham et al., 2005) and UCP2 (Pearce et al., 2003), which are mitochondrial anion carrier proteins that are involved in minimizing ROS emission from the electron transport chain (Mailloux and Harper, 2011).

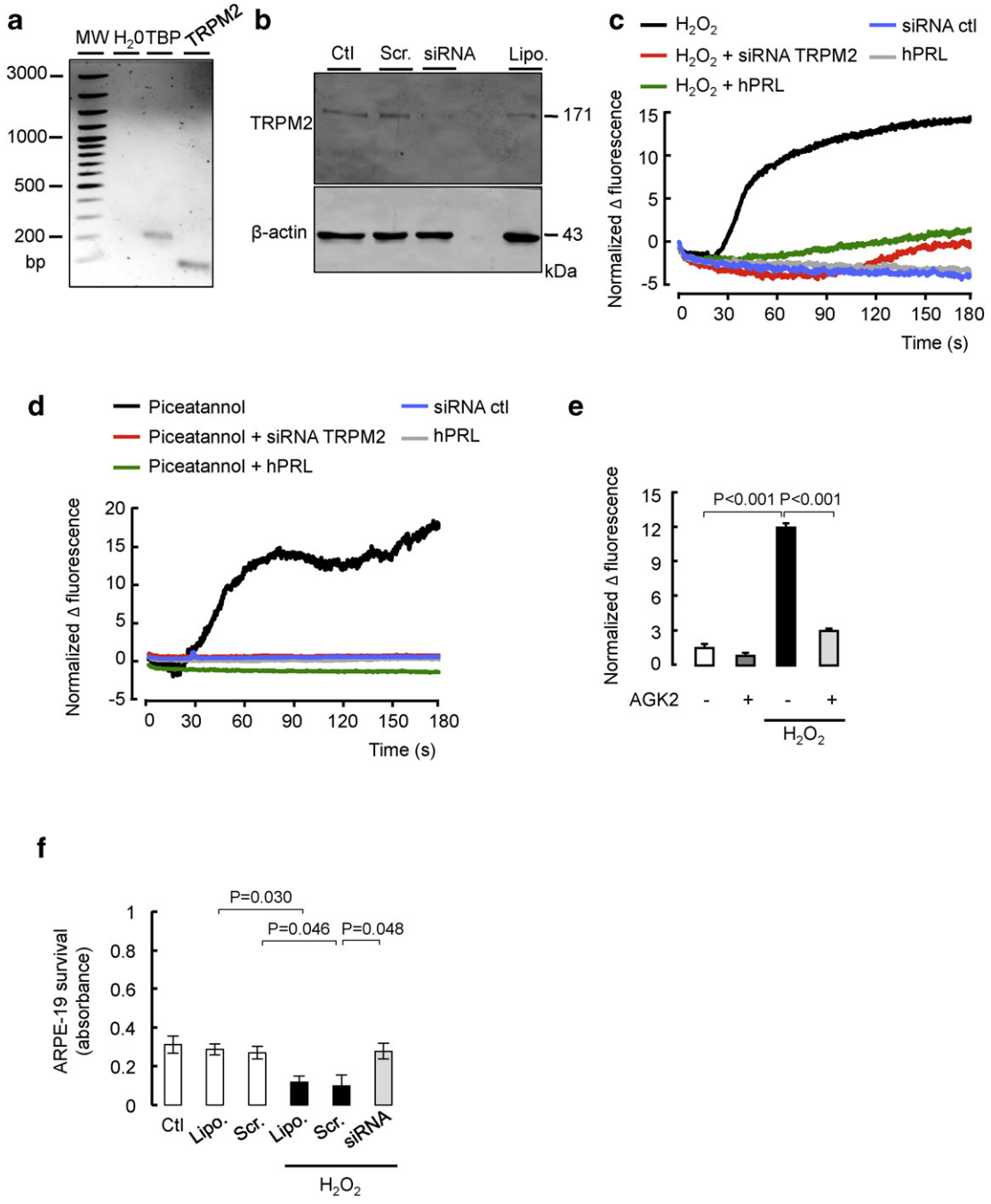

Fig. 5. PRL maintains human RPE cell survival by inhibiting the oxidant-induced SIRT2-dependent induction of TRPM2-mediated intracellular Ca^{2+} increase. (a) RT-PCR and (b) Western-blotting of TRPM2 in ARPE-19 cell lysates. (a) TBP was used as a positive control. bp, DNA ladder. RT-PCR was performed in RNA extracted from three independent cell cultures (N = 3). (b) ARPE-19 cells were untreated (Ctl), subjected to lipofectamin alone (Lipo.) or transfected with siRNA against TRPM2 (siRNA) or scramble sequence (Scr.). TRPM2 siRNA efficiently reduced TRPM2 expression as observed by immunoblotting using an anti-TRPM2 antibody that labeled a protein at the expected molecular weight for TRPM2 (171 kDa). β-Actin served as loading control. Extracts from three independent ARPE-19 cell cultures in each condition were analyzed (N = 3). (c, d) Measurement of the change in intracellular Ca^{2+} measured by the change in fluo-8 fluorescence (Δ fluorescence) in ARPE19 cells exposed to (c) H_2O_2 (100 μM) or (d) piceatannol (10 μM) while TRPM2 was blocked by siRNA against TRPM2 or PRL was applied (hPRL, 100 pmol/l, 15-min pretreatment). Scramble sequence (siRNA ctl) was used as a negative control for siRNA against TRPM2. Treatments with H_2O_2 or piceatannol began at time = 0 s (n = 170–190 cells; N = 3 independent replicates). (e) Ca^{2+}-dependent fluorescence change in ARPE19 cells 180 s after application of SIRT2 inhibitor AGK2 (10 μM) combined or not with H_2O_2 (100 μM) (n = 160–190 cells; N = 3 independent replicates). (f) Effect of TRPM2 inhibition on survival of ARPE-19 subjected to a 24-h H_2O_2 insult (100 μM) by MTT assay. ARPE-19 cells were untreated (Ctl), treated with lipofectamin alone (Lipo.) or transfected with siRNA against TRPM2 or the scramble sequence (Scr.) 24 h prior initiating the MTT assay. In (c–e), signals were normalized by subtracting the Fluo-8 Δ fluorescence to the one in untreated conditions. All bar plots, mean plus S.E.M.; *P* values: ANOVA and Bonferroni *post-hoc* test.

Consistent with previous studies (see review (Beatty et al., 2000)), here we show that H_2O_2 attenuated ARPE-19 cell survival by inhibiting their proliferation and stimulating their apoptosis, as evaluated by reduced ^{3}[H] incorporation and increased DNA fragmentation, respectively. Administering PRL before or after injury opposed the H_2O_2 cytotoxic and proapoptotic effect on ARPE-19 cells. The molecular mechanisms underlying this effect were not analyzed, but PRL is a well-known anti-apoptotic factor. It activates STAT3 (Adan et al., 2013), which signals to inhibit apoptosis by inducing Bcl-2 (Suemoto et al., 2007) and decreasing p53 (Adan et al., 2013) transcription. Reduced Bcl-2 contributes to RPE death by apoptosis, while pharmacologic treatments to block p53 expression can protect RPE cells from apoptosis (Bhattacharya et al., 2012).

The fact that PRL counteracts the proapoptotic effect of H_2O_2 argues in favor of its pro-survival effect on RPE under oxidative stress. Conversely, lack of PRL signaling should result in RPE apoptosis under pro-oxidant conditions. To investigate this concept, we studied the RPE in situ and chose advancing age as a model of RPE degeneration. Apoptosis occurred, but we did not observe any significant hypertrophy of RPE cells as others did in human tissue (Nag and Wadhwa, 2012). Notably, we showed that the levels of apoptosis were greater in the RPE of *prlr*$^{-/-}$ mice with advancing age than in the RPE of aged-matched wild-type mice or young *prlr*$^{-/-}$ mice. These data demonstrate the trophic effect of PRL on RPE *in vivo*. The antiapoptotic effect of PRL under challenging conditions was clearly established earlier (Marano and Ben-Jonathan, 2014). In particular, PRL protects beta cells *in vitro* from H_2O_2 (Yamamoto et al., 2010) and limits photoreceptor apoptosis in a phototoxicity model of retinal degeneration (Arnold et al., 2014).

PRL is essential for adult RPE survival. Targeted disruption of the PRL receptor gene causes apoptosis and reduces the number of RPE cells in this tissue, indicative of a defect in RPE survival, and also hypertrophy, which is known to lead to gradual atrophy (Nag and Wadhwa, 2012). Further supporting this notion is the fact that increased apoptosis and hypertrophy are observed in *prlr*$^{-/-}$ RPE independently of advancing age. Also, we show that immunoneutralization of PRL as well as a pure PRL receptor antagonist (Bernichtein et al., 2003) reduce ARPE-19 cell survival and proliferation, indicating that endogenous PRL is a major mitogenic factor for these cells.

A key issue is whether RPE is responding to local or circulating PRL, or both. Radioactive PRL injected intracardially is incorporated into ocular tissues (ciliary body, choroid, and retina) (O'Steen and Sundberg, 1982). The ciliary body is responsible for the active transport of plasma proteins to intraocular fluids (Mestriner and Haddad, 1997), and we demonstrated that the PRL receptor is localized in this structure (Arnold et al., 2010). To examine if the PRL receptor in the ciliary body could mediate uptake of circulating PRL, we analyzed retinal PRL in *prlr*$^{-/-}$ mice, which are known to be hyperprolactinemic (Schuff et al., 2002). The mice displayed 700-fold higher levels of circulating PRL (Arnold et al., 2010), but the levels of retinal PRL were similar to those of their wild-type littermates (Supplemental Fig. 5). A similar mechanism can also take place directly in the outer component of the blood-retina barrier, although this alternative warrants further investigation. If the exact contribution of local versus circulating PRL at RPE site needs further investigation, it is worth mentioning that both the estimated concentration of PRL in the conditioned media of ARPE-19 cultures and the dose of exogenously administered PRL are in the physiological range. PRL was previously shown to be necessary for cell survival in the absence of a challenging context in adult mice (Grosdemouge et al., 2003). Here, we demonstrate that a hormone is necessary for adult RPE survival. Such a conclusion had been reached previously only for antioxidant enzymes (Justilien et al., 2007) or transcription factors (Zhong et al., 2012).

A number of studies have demonstrated that oxidative injury in RPE cultures can be mitigated by compounds that exhibit antioxidant properties, including resveratrol (Chan et al., 2015). In contrast, we observed that piceatannol, a naturally occurring hydroxylated analog of resveratrol, promotes a sustained increase of intracellular Ca^{2+} that can cause apoptosis (Berridge et al., 2000) and reduces the survival of ARPE-19 cells. These data are consistent with a study showing that resveratrol and some of its analogs exert cytotoxic effects on normal nontransformed cells (She et al., 2003). Additionally, piceatannol has been previously associated with opposite effects on cell growth depending on its concentration, i.e., low doses (nM range) induce cell growth whereas high doses (μM range) attenuate cell growth (Vo et al., 2010).

Resveratrol and its analogs are substrate-specific activators of yeast and human sirtuins (Villalba and Alcain, 2012). Among the seven members of the mammalian sirtuin family, SIRT2 has been detected in adult retina (Geng et al., 2011), and disruption of its signaling has been proposed as an endogenous therapeutic target to preserve the integrity of aging cells against exogenous stressors such as ROS (Cheng et al., 2003). SIRT2 inhibition by AGK2 results in decreased ROS levels (Nie et al., 2014), which coincides with PRL decreasing intracellular levels of ROS in ARPE-19 cells. Consistent with studies showing that oxidative stress up-regulates SIRT2 (Nie et al., 2014), we found that both H_2O_2 exposure and advancing age cause the elevation of SIRT2 mRNA levels in ARPE-19 cells and mouse retinas, respectively. The fact that AGK2 decreases H_2O_2-induced apoptosis in ARPE-19 cells indicates that in these cells, SIRT2 mediates oxidative stress-induced apoptosis, as previously reported (Nie et al., 2014). Also, we show that PRL prevents the induction of SIRT2 expression under pro-oxidant conditions in ARPE-19 cells and that SIRT2 expression tends to be elevated in retinas from *prlr*$^{-/-}$ mice with advancing age compared to age-matched wild-type animals. Most conspicuously, SIRT2 expression was elevated in *prlr*$^{-/-}$ retinas from young mice. Considering that SIRT2 inactivates the PRL receptor through its deacetylation (Ma et al., 2010), our data suggest that a negative feed-back loop between SIRT2 and PRL signaling may exist. Together with the fact that PRL prevents the reduction in ARPE-19 cell survival induced by piceatannol, these data lead us to propose that PRL, by reducing ROS levels, maintains SIRT2 at levels that contribute to RPE survival. Conversely, under oxidizing conditions, increased levels of SIRT2 blunt PRL signaling, leading to RPE cell death. The possibility that PRL may directly regulate SIRT2 needs further studies.

Although PRL signaling, SIRT2, and TRPM2 channels are currently viewed as being independent, we suggest that these pathways are more intricately connected than previously appreciated. We report here that TRPM2 is expressed in ARPE-19 cells. This result complements a previous study showing that all TRP channel genes are expressed in the retina (Gilliam and Wensel, 2011). We also show that H_2O_2 activates TRPM2 leading to Ca^{2+} influx in a SIRT2-dependent manner since AGK2 blocks the H_2O_2-induced Ca^{2+} increase in ARPE-19 cells. In parallel, silencing TRPM2 inhibited the piceatannol-induced increase in intracellular Ca^{2+}, suggesting that SIRT2 increases intracellular Ca^{2+} by activating TRPM2. Thus, we assume that TRPM2 channels are activated by H_2O_2 in a SIRT2-dependent manner in ARPE-19 cells. Undoubtedly, the TRPM2-mediated Ca^{2+} rise is a dominant source of the Ca^{2+} required to reduce ARPE-19 cell viability under pro-oxidant conditions (Fig. 5f). Our observations are consistent with previous studies demonstrating that the TRPM2 Ca^{2+} current links oxidative stress-induced SIRT2 activation to oxidative stress-induced cell death (Faouzi and Penner, 2014).

The novelty here consists in demonstrating that PRL inhibits the oxidant-induced SIRT2-dependent activation of TRPM2 channels. PRL alone does not modify Ca^{2+} levels, and there is no evidence that PRL activates TRPM2. Instead, PRL seems to block TRPM2 once this latter is activated. We emphasize that this effect cannot be attributed to the ability of PRL to reduce SIRT2 transcription, because the time course of the two events is different (seconds/minutes versus 24 h). Reduced levels of intracellular ROS may explain the short-term effect of PRL on TRPM2 as well as the restorative effect of PRL at 6 h, though further studies using different techniques and dyes are required to address this issue. Interestingly, TRPM2 current density was shown to increase in cultured pyramidal neurons over time *in vitro*. This increase in current density

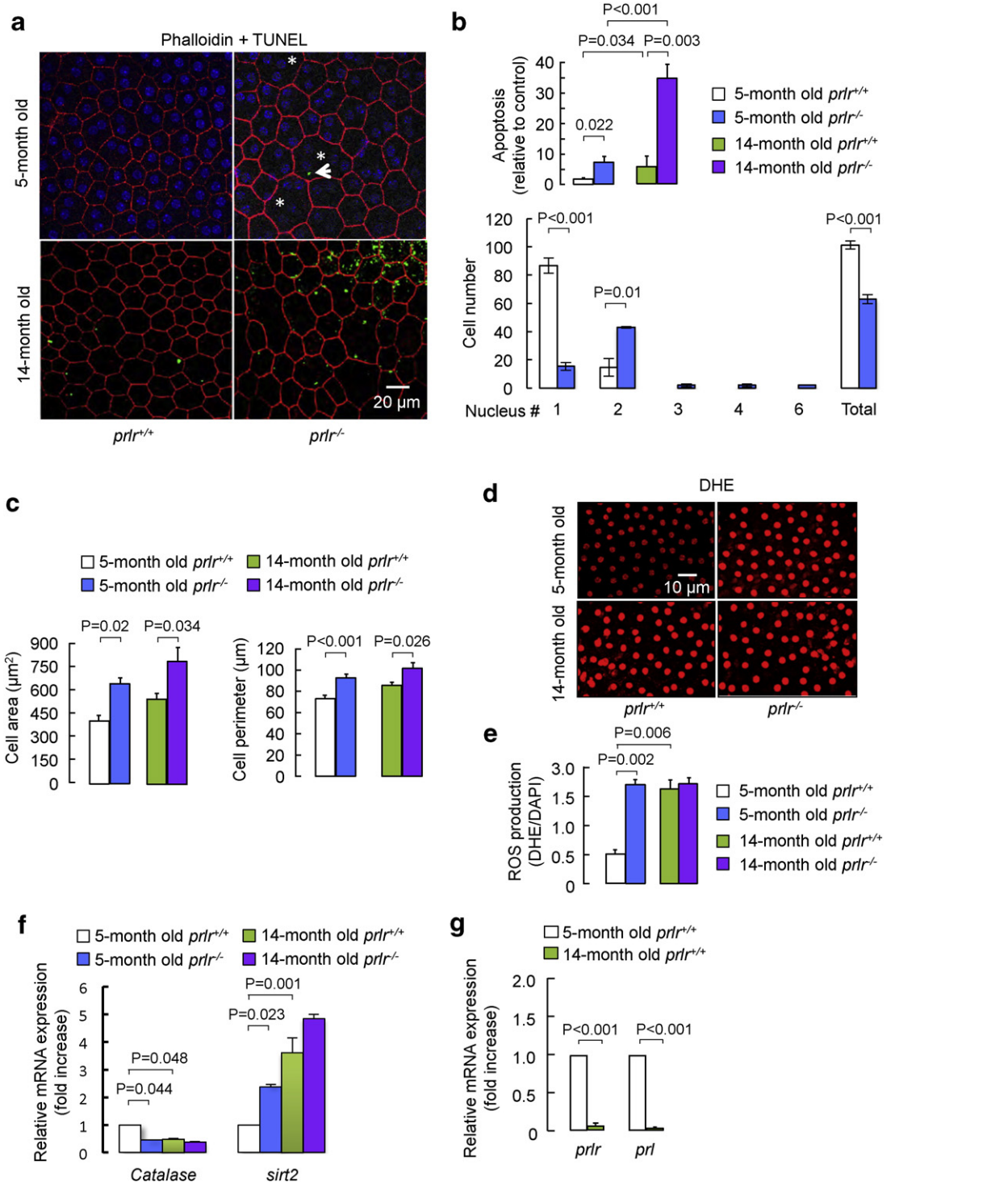

Fig. 6. RPE death in wild-type and PRL receptor-null mouse. (a) Representative stack image of TUNEL staining (green) in RPE flat-mounts of 5-month- and 14-month-old wild-type ($prlr^{+/+}$) and PRL receptor-null ($prlr^{-/-}$) mice in x-y axis. Rhodamine-phalloidin labeled F-actin (red), and DAPI labeled the nuclei (blue). Arrow indicates positive TUNEL stain and asterisks indicate morphological alterations. Corresponding separate images in x-y and z-axis projection were presented in Supplemental Fig. 4. Six sections per flat mount in three mice were observed. (b) Quantification of TUNEL-positive apoptosis signal in whole mounts of RPE (left upper panel; n = 4–11; N = 3 independent replicates). Quantification of cell number in RPE flat mounts from wild-type and $prlr^{-/-}$ mice. Data are presented as raw numbers (n = 4 sections of 200–200 μm per group from 6 flat mounts from 3 mice were analyzed). Note that no cell had 3, 4 or 6 nuclei in RPE flat mounts. (c) Averaged surface (right upper panel) and perimeter (right lower panel) of individual RPE cells from 5-month- and 14-month-old $prlr^{+/+}$ and $prlr^{-/-}$ mice. In (a–c), the 5-month-old $prlr^{+/+}$ and $prlr^{-/-}$ mouse group was composed of four males and three females and of three males and four females, respectively, while the 14-month-old $prlr^{+/+}$ and $prlr^{-/-}$ mouse group was composed of four males and two females and of three males and five females, respectively. (d) Representative images of superoxide anion production stained with DHE in RPE flat mounts of 5-month-old $prlr^{+/+}$ and $prlr^{-/-}$ mice, and of 14-month-old $prlr^{+/+}$ mice. (e) Quantification of fluorescence intensity as mean number of pixels positive for DHE staining normalized to the mean number of pixels positive for DAPI staining (not shown). Six sections per flat mount in three mice per group were observed. The 5-month-old $prlr^{+/+}$ and $prlr^{-/-}$ mouse group was composed of one male and two females, respectively, while the 14-month-old $prlr^{+/+}$ and $prlr^{-/-}$ mouse group was composed of two males and one female. (f) qRT-PCR analyses of catalase and SIRT2 mRNA in retina extracts of 5-month- and 14-month-old $prlr^{+/+}$ and $prlr^{-/-}$ mice. (g) qRT-PCR analyses of PRL receptor and PRL mRNA from retina extracts of 5-month- and 14-month-old $prlr^{+/+}$ and $prlr^{-/-}$ mice. All qRT-PCR data were normalized to TBP levels ($n = 6$ per genotype, 3 males and 3 females each; $N = 3$ independent replicates). Magnification bars as indicated. All bar plots, mean plus S.E.M. except in (b); *P* values: ANOVA and Bonferroni post-hoc test.

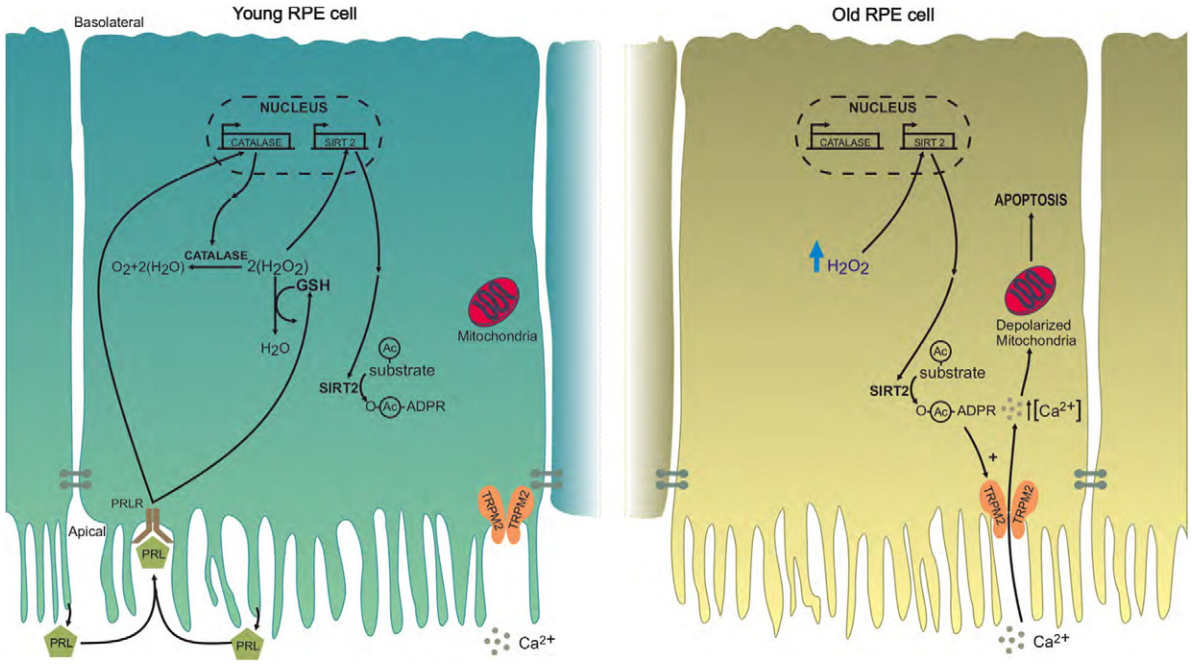

Fig. 7. Schematic depiction of the antiapoptotic conditions including the PRL signaling pathway in young RPE versus the proapoptotic conditions in aging RPE. Young RPE cells express PRL and its receptor (PRLR) that (1) signal for the synthesis of reduced glutathione (GSH) that transforms two molecules of hydrogen peroxide (H_2O_2) into water and (2) induces the transcription of catalase, which also processes H_2O_2 into water; both of these processes limit ROS levels. This antioxidant pathway is more prominent than the pro-oxidant pathway comprised by the TRPM2-mediated intracellular Ca^{2+} rise induced by the metabolite 2′O-acetyl-ADP-ribose (O-Ac-ADPR) that results from the deacetylation (removal of Ac group) of various substrates by SIRT2. The viability of RPE is therefore not jeopardized. In contrast, in aged RPE cells, the PRL signaling pathway is blunted. Therefore, the pro-oxidant pathway predominates over the antioxidant one. High levels of ROS, illustrated by increased H_2O_2, promote the up-regulation of SIRT2 which, in turn, activates TRPM2 by producing O-Ac-ADPR. The subsequent sustained rise in intracellular Ca^{2+} levels can depolarize mitochondria (Berridge et al., 2000), which causes apoptosis. RPE from PRLR null ($^{-/-}$) mice emphasizes these features.

was prevented by treatment with N-acetyl cysteine and conversely, depletion of GSH augmented TRPM2 currents (Lee et al., 2010).

Importantly, PRL is proteolytically cleaved in the retina to yield vasoinhibins (Clapp et al., 2006), a family of peptides that act on both endothelial and RPE cells to prevent the hypervasopermeability associated with diabetes (Arredondo Zamarripa et al., 2014). Vasoinhibins exert actions through a mechanism independent of the PRL receptor (Bajou et al., 2014). The existence of such mechanisms therefore makes the *prlr*$^{-/-}$ mouse a complex model since exaggerated signaling through non-PRL receptor pathways may be expected. However, we previously demonstrated that in spite of being hyperprolactinemic, *prlr*$^{-/-}$ mice do not show increased levels of vasoinhibins in their retinas (Arnold et al., 2010).

Our general view is that antiapoptotic mechanisms including the PRL signaling pathway degrade with advancing age so that RPE cells become vulnerable to normal proapoptotic stressors such as ROS, SIRT2, and elevated intracellular Ca^{2+} levels, creating a tipping point beyond which retinal homeostasis is lost (Fig. 7), leading to visual dysfunction as we previously reported (Arnold et al., 2014). Concomitantly with RPE damage, rhodopsin mRNA levels and cone and rod photoreception are compromised in the prlr$^{-/-}$ mice (Arnold et al., 2014). A similar degree of alterations in electroretinogram parameters was previously shown to associate with reduced visual acuity in various animal models (Bonnet Wersinger et al., 2014; Deming et al., 2015; Hilgen et al., 2012; Kohl et al., 2015).

Most studies devoted to detecting changes in plasma levels of PRL during aging in humans have been carried out in males, usually with age-range subject selection, which results in considerable variability and conflicting results. In most studies, healthy aging subjects showed no change in circulating levels of pituitary PRL (Rossmanith et al., 1992; Schiavi et al., 1992; Yamaji et al., 1976), while some showed a decrease (Saucedo et al., 2000; van Coevorden et al., 1991). From a clinical point of view, one may consider the option of increasing levels of systemic PRL during advancing age in order to protect the RPE. However, the potential undesirable effects of induced hyperprolactinemia prompt us to propose instead that targeting SIRT2 or TRPM2 channels with inhibitors may improve RPE function in conditions that induce oxidative stress in the RPE. Therapeutic interventions may also benefit from identifying the signal transduction pathways that link PRL receptor stimulation to antioxidant actions. STAT3 appears to be a main candidate since signaling through the PRL receptor canonically involves JAK2/STAT3 activation (Bole-Feysot et al., 1998), and neuronal oxidative stress associates with reduced JAK2/STAT signaling (Kaur et al., 2005; Monroe and Halvorsen, 2006a), an effect that can be counteracted by anti-oxidant molecules including GSH and NAC (Monroe and Halvorsen, 2006b). In particular, knockdown of STAT3 has been recently shown to abolish the protective effects of innate immune system activation in the retina during oxidative stress (Patel and Hackam, 2014), and PRL is a well-known modulator of this system (Díaz et al., 2013).

Author Contributions

Conceived and designed the experiments: ST, EA, and CC. Performed the experiments: RMG, DAZ, EA, XRH, RNI, JRE, GBC, NA, BO, and ST. Analyzed the data: RMG, DAZ, BO, and ST. Interpreted the data: FPO, ATM, CC, and ST. Contributed reagents/materials/analysis tools: FPO, NB, VG, ATM, CC, and ST. Wrote the paper: ST.

Conflict of Interest Statement

The authors declare no competing financial interests.

Acknowledgements

We would like to thank M. Diaz Muñoz and M. Flourakis for insights. R. Meléndez García, D. Arredondo Zamarripa, E. Arnold, X. Ruiz-Herrera, G. Baeza Cruz, and N. Adán are Master's and Doctoral students from Programa de Posgrado en Ciencias, Universidad Nacional Autónoma de

México (UNAM) and received fellowships from CONACYT. We thank F. López-Barrera, G. Nava, D. Mondragón, A. Prado, M. García, and E. N. Hernández Ríos for their technical assistance, and D. D. Pless for critically editing the manuscript. This study was supported by the UNAM grant IN201814 (ST), the National Council of Science and Technology of Mexico (CONACYT) grant 176393 (ST), and the Shedid grant (ATM). The role of the three funders strictly consisted in providing funds to purchase all materials necessary in this study.

Appendix A. Supplementary data

Supplementary data to this article can be found online at http://dx.doi.org/10.1016/j.ebiom.2016.03.048.

References

Adan, N., Guzman-Morales, J., Ledesma-Colunga, M.G., Perales-Canales, S.I., Quintanar-Stephano, A., Lopez-Barrera, F., Mendez, I., Moreno-Carranza, B., Triebel, J., Binart, N., et al., 2013. Prolactin promotes cartilage survival and attenuates inflammation in inflammatory arthritis. J. Clin. Invest. 123, 3902–3913.

Ambati, J., Ambati, B.K., Yoo, S.H., Ianchulev, S., Adamis, A.P., 2003. Age-related macular degeneration: etiology, pathogenesis, and therapeutic strategies. Surv. Ophthalmol. 48, 257–293.

Ardeljan, D., Chan, C.C., 2013. Aging is not a disease: distinguishing age-related macular degeneration from aging. Prog. Retin. Eye Res. 37, 68–89.

Arnold, E., Rivera, J.C., Thebault, S., Moreno-Paramo, D., Quiroz-Mercado, H., Quintanar-Stephano, A., Binart, N., Martinez de la Escalera, G., Clapp, C., 2010. High levels of serum prolactin protect against diabetic retinopathy by increasing ocular vasoinhibins. Diabetes 59, 3192–3197.

Arnold, E., Thebault, S., Baeza-Cruz, G., Arredondo Zamarripa, D., Adan, N., Quintanar-Stephano, A., Condes-Lara, M., Rojas-Piloni, G., Binart, N., Martinez de la Escalera, G., et al., 2014. The hormone prolactin is a novel, endogenous trophic factor able to regulate reactive glia and to limit retinal degeneration. J. Neurosci. 34, 1868–1878.

Arredondo Zamarripa, D., Diaz-Lezama, N., Melendez Garcia, R., Chavez Balderas, J., Adan, N., Ledesma-Colunga, M.G., Arnold, E., Clapp, C., Thebault, S., 2014. Vasoinhibins regulate the inner and outer blood-retinal barrier and limit retinal oxidative stress. Front. Cell. Neurosci. 8, 333.

Bajou, K., Herkenne, S., Thijssen, V.L., D'Amico, S., Nguyen, N.Q., Bouche, A., Tabruyn, S., Srahna, M., Carabin, J.Y., Nivelles, O., et al., 2014. PAI-1 mediates the antiangiogenic and profibrinolytic effects of 16K prolactin. Nat. Med. 20, 741–747.

Balaban, R.S., Nemoto, S., Finkel, T., 2005. Mitochondria, oxidants, and aging. Cell 120, 483–495.

Beatty, S., Koh, H., Phil, M., Henson, D., Boulton, M., 2000. The role of oxidative stress in the pathogenesis of age-related macular degeneration. Surv. Ophthalmol. 45, 115–134.

Bernichtein, S., Kayser, C., Dillner, K., Moulin, S., Kopchick, J.J., Martial, J.A., Norstedt, G., Isaksson, O., Kelly, P.A., Goffin, V., 2003. Development of pure prolactin receptor antagonists. J. Biol. Chem. 278, 35988–35999.

Berridge, M.J., Lipp, P., Bootman, M.D., 2000. The versatility and universality of calcium signalling. Nat. Rev. Mol. Cell Biol. 1, 11–21.

Bhattacharya, S., Chaum, E., Johnson, D.A., Johnson, L.R., 2012. Age-related susceptibility to apoptosis in human retinal pigment epithelial cells is triggered by disruption of p53-Mdm2 association. Invest. Ophthalmol. Vis. Sci. 53, 8350–8366.

Bispham, J., Gardner, D.S., Gnanalingham, M.G., Stephenson, T., Symonds, M.E., Budge, H., 2005. Maternal nutritional programming of fetal adipose tissue development: differential effects on messenger ribonucleic acid abundance for uncoupling proteins and peroxisome proliferator-activated and prolactin receptors. Endocrinology 146, 3943–3949.

Bole-Feysot, C., Goffin, V., Edery, M., Binart, N., Kelly, P.A., 1998. Prolactin (PRL) and its receptor: actions, signal transduction pathways and phenotypes observed in PRL receptor knockout mice. Endocr. Rev. 19, 225–268.

Bolzan, A.D., Brown, O.A., Goya, R.G., Bianchi, M.S., 1995. Hormonal modulation of antioxidant enzyme activities in young and old rats. Exp. Gerontol. 30, 169–175.

Bonnet Wersinger, D., Benkafadar, N., Jagodzinska, J., Hamel, C., Tanizawa, Y., Lenaers, G., Delettre, C., 2014. Impairment of visual function and retinal ER stress activation in Wfs1-deficient mice. PLoS One 9, e97222.

Broadhead, G.K., Grigg, J.R., Chang, A.A., McCluskey, P., 2015. Dietary modification and supplementation for the treatment of age-related macular degeneration. Nutr. Rev. 73, 448–462.

Brown-Borg, H.M., Bode, A.M., Bartke, A., 1999. Antioxidative mechanisms and plasma growth hormone levels: potential relationship in the aging process. Endocrine 11, 41–48.

Camandola, S., Mattson, M.P., 2011. Aberrant subcellular neuronal calcium regulation in aging and Alzheimer's disease. Biochim. Biophys. Acta 1813, 965–973.

Castilla, A., Garcia, C., Cruz-Soto, M., Martinez de la Escalera, G., Thebault, S., Clapp, C., 2010. Prolactin in ovarian follicular fluid stimulates endothelial cell proliferation. J. Vasc. Res. 47, 45–53.

Chan, C.M., Huang, C.H., Li, H.J., Hsiao, C.Y., Su, C.C., Lee, P.L., Hung, C.F., 2015. Protective effects of resveratrol against UVA-induced damage in ARPE19 cells. Int. J. Mol. Sci. 16, 5789–5802.

Cheng, H.L., Mostoslavsky, R., Saito, S., Manis, J.P., Gu, Y., Patel, P., Bronson, R., Appella, E., Alt, F.W., Chua, K.F., 2003. Developmental defects and p53 hyperacetylation in Sir2 homolog (SIRT1)-deficient mice. Proc. Natl. Acad. Sci. U. S. A. 100, 10794–10799.

Clapp, C., Aranda, J., Gonzalez, C., Jeziorski, M.C., Martinez de la Escalera, G., 2006. Vasoinhibins: endogenous regulators of angiogenesis and vascular function. Trends Endocrinol. Metab. 17, 301–307.

Claybon, A., Bishop, A.J., 2011. Dissection of a mouse eye for a whole mount of the retinal pigment epithelium. J. Vis. Exp.

Cross, C.E., Halliwell, B., Borish, E.T., Pryor, W.A., Ames, B.N., Saul, R.L., McCord, J.M., Harman, D., 1987. Oxygen radicals and human disease. Ann. Intern. Med. 107, 526–545.

De Luca Brunori, I., Moggi, G., Fornaro, P., Teti, G., Murru, S., Gadducci, A., Castrogiovanni, P., Perossini, M., 1985. Evaluation of the central dopaminergic activity in gestational hyperprolactinaemia by means of the electroretinographic technique. Clin. Exp. Obstet. Gynecol. 12, 13–15.

Deming, J.D., Pak, J.S., Brown, B.M., Kim, M.K., Aung, M.H., Eom, Y.S., Shin, J.A., Lee, E.J., Pardue, M.T., Craft, C.M., 2015. Visual cone arrestin 4 contributes to visual function and cone health. Invest. Ophthalmol. Vis. Sci. 56, 5407–5416.

Díaz, L., Díaz Muñoz, M., González, L., Lira-Albarrán, S., Larrea, F., Méndez, I., 2013. Prolactin in the immune system. Medicine "Obstetrics and Gynecology" "Prolactin" Chapter 4.

Du, Y., Veenstra, A., Palczewski, K., Kern, T.S., 2013. Photoreceptor cells are major contributors to diabetes-induced oxidative stress and local inflammation in the retina. Proc. Natl. Acad. Sci. U. S. A. 110, 16586–16591.

Duckles, S.P., Miller, V.M., 2010. Hormonal modulation of endothelial NO production. Pflugers Arch. 459, 841–851.

Dunn, K.C., Aotaki-Keen, A.E., Putkey, F.R., Hjelmeland, L.M., 1996. ARPE-19, a human retinal pigment epithelial cell line with differentiated properties. Exp. Eye Res. 62, 155–169.

Faouzi, M., Penner, R., 2014. Trpm2. Handb. Exp. Pharmacol. 222, 403–426.

Finkel, T., Holbrook, N.J., 2000. Oxidants, oxidative stress and the biology of ageing. Nature 408, 239–247.

Freeman, M.E., Kanyicska, B., Lerant, A., Nagy, G., 2000. Prolactin: structure, function, and regulation of secretion. Physiol. Rev. 80, 1523–1631.

Geng, Y., Wang, J., Liang, J., Xu, C., Zhi, Y., 2011. Expression of Sirt1 and Sirt2 in injured optic retina of calorie restricted rats. Eye Sci. 26, 221–224.

Gill, M.T., Bajaj, R., Chang, C.J., Nichols, D.E., McLaughlin, J.L., 1987. 3,3′,5′-Tri-O-methylpiceatannol and 4.3′,5′-tri-O-methylpiceatannol: improvements over piceatannol in bioactivity. J. Nat. Prod. 50, 36–40.

Gilliam, J.C., Wensel, T.G., 2011. TRP channel gene expression in the mouse retina. Vis. Res. 51, 2440–2452.

Grosdemouge, I., Bachelot, A., Lucas, A., Baran, N., Kelly, P.A., Binart, N., 2003. Effects of deletion of the prolactin receptor on ovarian gene expression. Reprod. Biol. Endocrinol. 1, 12.

Grubisha, O., Rafty, L.A., Takanishi, C.L., Xu, X., Tong, L., Perraud, A.L., Scharenberg, A.M., Denu, J.M., 2006. Metabolite of SIR2 reaction modulates TRPM2 ion channel. J. Biol. Chem. 281, 14057–14065.

Hall, J.A., Dominy, J.E., Lee, Y., Puigserver, P., 2013. The sirtuin family's role in aging and age-associated pathologies. J. Clin. Invest. 123, 973–979.

Hamel, C.P., Tsilou, E., Pfeffer, B.A., Hooks, J.J., Detrick, B., Redmond, T.M., 1993. Molecular cloning and expression of RPE65, a novel retinal pigment epithelium-specific microsomal protein that is post-transcriptionally regulated in vitro. J. Biol. Chem. 268, 15751–15757.

He, Y., Leung, K.W., Ren, Y., Pei, J., Ge, J., Tombran-Tink, J., 2014. PEDF improves mitochondrial function in RPE cells during oxidative stress. Invest. Ophthalmol. Vis. Sci. 55, 6742–6755.

Hilgen, G., Huebner, A.K., Tanimoto, N., Sothilingam, V., Seide, C., Garcia Garrido, M., Schmidt, K.F., Seeliger, M.W., Lowel, S., Weiler, R., et al., 2012. Lack of the sodium-driven chloride bicarbonate exchanger NCBE impairs visual function in the mouse retina. PLoS One 7, e46155.

Howitz, K.T., Bitterman, K.J., Cohen, H.Y., Lamming, D.W., Lavu, S., Wood, J.G., Zipkin, R.E., Chung, P., Kisielewski, A., Zhang, L.L., et al., 2003. Small molecule activators of sirtuins extend *Saccharomyces cerevisiae* lifespan. Nature 425, 191–196.

Justilien, V., Pang, J.J., Renganathan, K., Zhan, X., Crabb, J.W., Kim, S.R., Sparrow, J.R., Hauswirth, W.W., Lewin, A.S., 2007. SOD2 knockdown mouse model of early AMD. Invest. Ophthalmol. Vis. Sci. 48, 4407–4420.

Kaur, N., Lu, B., Monroe, R.K., Ward, S.M., Halvorsen, S.W., 2005. Inducers of oxidative stress block ciliary neurotrophic factor activation of Jak/STAT signaling in neurons. J. Neurochem. 92, 1521–1530.

Kerksick, C., Willoughby, D., 2005. The antioxidant role of glutathione and N-acetyl-cysteine supplements and exercise-induced oxidative stress. J. Int. Soc. Sports Nutr. 2, 38–44.

Kohl, S., Zobor, D., Chiang, W.C., Weisschuh, N., Staller, J., Gonzalez Menendez, I., Chang, S., Beck, S.C., Garcia Garrido, M., Sothilingam, V., et al., 2015. Mutations in the unfolded protein response regulator ATF6 cause the cone dysfunction disorder achromatopsia. Nat. Genet. 47, 757–765.

Lee, M., Cho, T., Jantaratnotai, N., Wang, Y.T., McGeer, E., McGeer, P.L., 2010. Depletion of GSH in glial cells induces neurotoxicity: relevance to aging and degenerative neurological diseases. FASEB J. 24, 2533–2545.

Ma, L., Gao, J.S., Guan, Y., Shi, X., Zhang, H., Ayrapetov, M.K., Zhang, Z., Xu, L., Hyun, Y.M., Kim, M., et al., 2010. Acetylation modulates prolactin receptor dimerization. Proc. Natl. Acad. Sci. U. S. A. 107, 19314–19319.

Mailloux, R.J., Harper, M.E., 2011. Uncoupling proteins and the control of mitochondrial reactive oxygen species production. Free Radic. Biol. Med. 51, 1106–1115.

Marano, R.J., Ben-Jonathan, N., 2014. Minireview: extrapituitary prolactin: an update on the distribution, regulation, and functions. Mol. Endocrinol. 28, 622–633.

Mennicke, W.H., Kral, T., Krumbiegel, G., Rittmann, N., 1987. Determination of N-acetyl-S-(N-alkylthiocarbamoyl)-L-cysteine, a principal metabolite of alkyl isothiocyanates, in rat urine. J. Chromatogr. 414, 19–24.
Mestriner, A.C., Haddad, A., 1997. Horseradish peroxidase: a reliable or a misleading tool for the investigations on the origin of the proteins of the aqueous humor? Cell Tissue Res. 289, 85–96.
Miceli, M.V., Liles, M.R., Newsome, D.A., 1994. Evaluation of oxidative processes in human pigment epithelial cells associated with retinal outer segment phagocytosis. Exp. Cell Res. 214, 242–249.
Minoo, P., Zadeh, M.M., Rottapel, R., Lebrun, J.J., Ali, S., 2004. A novel SHP-1/Grb2-dependent mechanism of negative regulation of cytokine-receptor signaling: contribution of SHP-1 C-terminal tyrosines in cytokine signaling. Blood 103, 1398–1407.
Monroe, R.K., Halvorsen, S.W., 2006a. Cadmium blocks receptor-mediated Jak/STAT signaling in neurons by oxidative stress. Free Radic. Biol. Med. 41, 493–502.
Monroe, R.K., Halvorsen, S.W., 2006b. Mercury abolishes neurotrophic factor-stimulated Jak-STAT signaling in nerve cells by oxidative stress. Toxicol. Sci. 94, 129–138.
Morales, T., 2011. Recent findings on neuroprotection against excitotoxicity in the hippocampus of female rats. J. Neuroendocrinol. 23, 994–1001.
Mustafi, D., Maeda, T., Kohno, H., Nadeau, J.H., Palczewski, K., 2012. Inflammatory priming predisposes mice to age-related retinal degeneration. J. Clin. Invest. 122, 2989–3001.
Nag, T.C., Wadhwa, S., 2012. Ultrastructure of the human retina in aging and various pathological states. Micron 43, 759–781.
Nandrot, E.F., Chang, Y., Finnemann, S.C., 2008. Alphavbeta5 integrin receptors at the apical surface of the RPE: one receptor, two functions. Adv. Exp. Med. Biol. 613, 369–375.
Nie, H., Hong, Y., Lu, X., Zhang, J., Chen, H., Li, Y., Ma, Y., Ying, W., 2014. SIRT2 mediates oxidative stress-induced apoptosis of differentiated PC12 cells. Neuroreport.
Organisciak, D.T., Vaughan, D.K., 2010. Retinal light damage: mechanisms and protection. Prog. Retin. Eye Res. 29, 113–134.
Ormandy, C.J., Camus, A., Barra, J., Damotte, D., Lucas, B., Buteau, H., Edery, M., Brousse, N., Babinet, C., Binart, N., et al., 1997. Null mutation of the prolactin receptor gene produces multiple reproductive defects in the mouse. Genes Dev. 11, 167–178.
O'Steen, W.K., Sundberg, D.K., 1982. Patterns of radioactivity in the eyes of rats after injection of iodinated prolactin. Ophthalmic Res. 14, 54–62.
Ovey, I.S., Naziroglu, M., 2015. Homocysteine and cytosolic GSH depletion induce apoptosis and oxidative toxicity through cytosolic calcium overload in the hippocampus of aged mice: involvement of TRPM2 and TRPV1 channels. Neuroscience 284, 225–233.
Pallos, J., Bodai, L., Lukacsovich, T., Purcell, J.M., Steffan, J.S., Thompson, L.M., Marsh, J.L., 2008. Inhibition of specific HDACs and sirtuins suppresses pathogenesis in a *Drosophila* model of Huntington's disease. Hum. Mol. Genet. 17, 3767–3775.
Patel, A.K., Hackam, A.S., 2014. A novel protective role for the innate immunity Toll-Like Receptor 3 (TLR3) in the retina via Stat3. Mol. Cell. Neurosci. 63, 38–48.
Pearce, S., Mostyn, A., Alves-Guerra, M.C., Pecqueur, C., Miroux, B., Webb, R., Stephenson, T., Symond, M.E., 2003. Prolactin, prolactin receptor and uncoupling proteins during fetal and neonatal development. Proc. Nutr. Soc. 62, 421–427.
Pena, F., Ordaz, B., 2008. Non-selective cation channel blockers: potential use in nervous system basic research and therapeutics. Mini-Rev. Med. Chem. 8, 812–819.
Piotrowska, H., Kucinska, M., Murias, M., 2012. Biological activity of piceatannol: leaving the shadow of resveratrol. Mutat. Res. 750, 60–82.
Ramirez, M., Hernandez-Montoya, J., Sanchez-Serrano, S.L., Ordaz, B., Ferraro, S., Quintero, H., Pena-Ortega, F., Lamas, M., 2012. GABA-mediated induction of early neuronal markers expression in postnatal rat progenitor cells in culture. Neuroscience 224, 210–222.
Rebrin, I., Forster, M.J., Sohal, R.S., 2007. Effects of age and caloric intake on glutathione redox state in different brain regions of C57BL/6 and DBA/2 mice. Brain Res. 1127, 10–18.
Ricke-Hoch, M., Bultmann, I., Stapel, B., Condorelli, G., Rinas, U., Sliwa, K., Scherr, M., Hilfiker-Kleiner, D., 2014. Opposing roles of Akt and STAT3 in the protection of the maternal heart from peripartum stress. Cardiovasc. Res. 101, 587–596.
Rivera, J.C., Aranda, J., Riesgo, J., Nava, G., Thebault, S., Lopez-Barrera, F., Ramirez, M., Martinez de la Escalera, G., Clapp, C., 2008. Expression and cellular localization of prolactin and the prolactin receptor in mammalian retina. Exp. Eye Res. 86, 314–321.
Rossmanith, W.G., Szilagyi, A., Scherbaum, W.A., 1992. Episodic thyrotropin (TSH) and prolactin (PRL) secretion during aging in postmenopausal women. Horm. Metab. Res. 24, 185–190.
Saucedo, R.P., Fonseca, M.E., Basurto, L., Ochoa, R., Sanchez, M., Zarate, A., 2000. Decrease in circulating androgens in men during senescence. Gac. Med. Mex. 136, 335–339.
Schiavi, R.C., White, D., Mandeli, J., 1992. Pituitary-gonadal function during sleep in healthy aging men. Psychoneuroendocrinology 17, 599–609.
Schuff, K.G., Hentges, S.T., Kelly, M.A., Binart, N., Kelly, P.A., Iuvone, P.M., Asa, S.L., Low, M.J., 2002. Lack of prolactin receptor signaling in mice results in lactotroph proliferation and prolactinomas by dopamine-dependent and -independent mechanisms. J. Clin. Invest. 110, 973–981.
She, Q.B., Ma, W.Y., Wang, M., Kaji, A., Ho, C.T., Dong, Z., 2003. Inhibition of cell transformation by resveratrol and its derivatives: differential effects and mechanisms involved. Oncogene 22, 2143–2150.
Shen, J.K., Dong, A., Hackett, S.F., Bell, W.R., Green, W.R., Campochiaro, P.A., 2007. Oxidative damage in age-related macular degeneration. Histol. Histopathol. 22, 1301–1308.
Sparrow, J.R., Hicks, D., Hamel, C.P., 2010. The retinal pigment epithelium in health and disease. Curr. Mol. Med. 10, 802–823.
Stohr, M., Eipel, H., Goerttler, K., Vogt-Schaden, M., 1977. Extended application of flow microfluorometry by means of dual laser excitation. Histochemistry 51, 305–313.
Suemoto, H., Muragaki, Y., Nishioka, K., Sato, M., Ooshima, A., Itoh, S., Hatamura, I., Ozaki, M., Braun, A., Gustafsson, E., et al., 2007. Trps1 regulates proliferation and apoptosis of chondrocytes through Stat3 signaling. Dev. Biol. 312, 572–581.
Swaroop, A., Chew, E.Y., Rickman, C.B., Abecasis, G.R., 2009. Unraveling a multifactorial late-onset disease: from genetic susceptibility to disease mechanisms for age-related macular degeneration. Annu. Rev. Genomics Hum. Genet. 10, 19–43.
Takahashi, N., Kozai, D., Kobayashi, R., Ebert, M., Mori, Y., 2011. Roles of TRPM2 in oxidative stress. Cell Calcium 50, 279–287.
Tallet, E., Fernandez, I., Zhang, C., Salsac, M., Gregor, N., Ayoub, M.A., Pin, J.P., Trinquet, E., Goffin, V., 2011. Investigation of prolactin receptor activation and blockade using time-resolved fluorescence resonance energy transfer. Front. Endocrinol. (Lausanne) 2, 29.
Toescu, E.C., Verkhratsky, A., Landfield, P.W., 2004. Ca^{2+} regulation and gene expression in normal brain aging. Trends Neurosci. 27, 614–620.
Tong, L., Denu, J.M., 2010. Function and metabolism of sirtuin metabolite O-acetyl-ADP-ribose. Biochim. Biophys. Acta 1804, 1617–1625.
van Coevorden, A., Mockel, J., Laurent, E., Kerkhofs, M., L'Hermite-Baleriaux, M., Decoster, C., Neve, P., Van Cauter, E., 1991. Neuroendocrine rhythms and sleep in aging men. Am. J. Phys. 260, E651–E661.
Villalba, J.M., Alcain, F.J., 2012. Sirtuin activators and inhibitors. Biofactors 38, 349–359.
Vo, N.T., Madlener, S., Bago-Horvath, Z., Herbacek, I., Stark, N., Gridling, M., Probst, P., Giessrigl, B., Bauer, S., Vonach, C., et al., 2010. Pro- and anticarcinogenic mechanisms of piceatannol are activated dose dependently in MCF-7 breast cancer cells. Carcinogenesis 31, 2074–2081.
Wei, C.X., Sun, A., Yu, Y., Liu, Q., Tan, Y.Q., Tachibana, I., Zeng, H., Wei, J.Y., 2016. Challenges in the development of therapy for dry age-related macular degeneration. Adv. Exp. Med. Biol. 854, 103–109.
Yamaji, T., Shimamoto, K., Ishibashi, M., Kosaka, K., Orimo, H., 1976. Effect of age and sex on circulating and pituitary prolactin levels in human. Acta Endocrinol. 83, 711–719.
Yamamoto, T., Mita, A., Ricordi, C., Messinger, S., Miki, A., Sakuma, Y., Timoneri, F., Barker, S., Fornoni, A., Molano, R.D., et al., 2010. Prolactin supplementation to culture medium improves beta-cell survival. Transplantation 89, 1328–1335.
Yuksel, M., Naziroglu, M., Ozkaya, M.O., 2015. Long-term exposure to electromagnetic radiation from mobile phones and Wi-Fi devices decreases plasma prolactin, progesterone, and estrogen levels but increases uterine oxidative stress in pregnant rats and their offspring. Endocrine.
Yu-Lee, L.Y., 2002. Prolactin modulation of immune and inflammatory responses. Recent Prog. Horm. Res. 57, 435–455.
Zhao, Z., Chen, Y., Wang, J., Sternberg, P., Freeman, M.L., Grossniklaus, H.E., Cai, J., 2011. Age-related retinopathy in NRF2-deficient mice. PLoS One 6, e19456.
Zheng, W., 2013. Mechanism-based modulator discovery for sirtuin-catalyzed deacetylation reaction. Mini-Rev. Med. Chem. 13, 132–154.
Zhong, Y., Li, J., Wang, J.J., Chen, C., Tran, J.T., Saadi, A., Yu, Q., Le, Y.Z., Mandal, M.N., Anderson, R.E., et al., 2012. X-box binding protein 1 is essential for the anti-oxidant defense and cell survival in the retinal pigment epithelium. PLoS One 7, e38616.